

AD-A121 948

THE AFGL IMAGE RECONSTRUCTION PROGRAM II SPECKLE  
INTERFEROMETRY (U) AIR FORCE GEOPHYSICS LAB HANSCOM AFB  
MA S P WORDEN ET AL. 01 DEC 81 AFGL-TR-82-0341

1/1

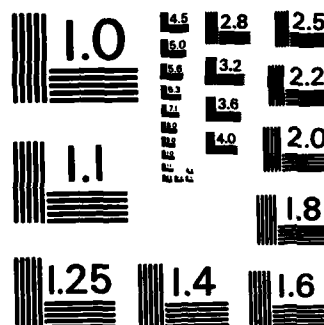
UNCLASSIFIED

F/G 20/6.

NL

END

FILED  
+  
1074



MICROCOPY RESOLUTION TEST CHART  
NATIONAL BUREAU OF STANDARDS-1963-A

Unclassified

SECURITY CLASSIFICATION OF THIS PAGE (When Data Entered)

REPORT DOCUMENTATION PAGE		READ INSTRUCTIONS BEFORE COMPLETING FORM
1. REPORT NUMBER AFGL-TR-82-0341	2. GOVT ACCESSION NO. AD A121940	3. RECIPIENT'S CATALOG NUMBER
4. TITLE (and Subtitle) The AFGL Image Reconstruction Program II Speckle Interferometry		5. TYPE OF REPORT & PERIOD COVERED REPRINT
		6. PERFORMING ORG. REPORT NUMBER
7. AUTHOR(s) Simon P. Worden, Capt, USAF N. J. Woolf* E.K. Hege* P. A. Strittmatter* E.N. Hubbard*		8. CONTRACT OR GRANT NUMBER(s)
9. PERFORMING ORGANIZATION NAME AND ADDRESS Air Force Geophysics Laboratory (PHS) Hanscom AFB Massachusetts 01731		10. PROGRAM ELEMENT, PROJECT, TASK AREA & WORK UNIT NUMBERS 61102F 2311G317
11. CONTROLLING OFFICE NAME AND ADDRESS Air Force Geophysics Laboratory (PHG) Hanscom AFB Massachusetts 01731		12. REPORT DATE 18 November 1982
		13. NUMBER OF PAGES 62
14. MONITORING AGENCY NAME & ADDRESS (if different from Controlling Office)		15. SECURITY CLASS. (of this report) Unclassified
		15a. DECLASSIFICATION/DOWNGRADING SCHEDULE
16. DISTRIBUTION STATEMENT (of this Report) Approved for public release; distribution unlimited.		
17. DISTRIBUTION STATEMENT (of the abstract entered in Block 20, if different from Report) B		
18. SUPPLEMENTARY NOTES *Steward Observatory, The University of Arizona Reprinted from AFSC Space Division (SD-TR-82-45), 1 December 1981, Final Report, pp 1-59		
19. KEY WORDS (Continue on reverse side if necessary and identify by block number) Satellite imagery Speckle interferometry		
20. ABSTRACT (Continue on reverse side if necessary and identify by block number) Recent work indicates that large-telescope, optics-limited images are recoverable for objects as faint as +15 stellar magnitudes using a technique called speckle interferometry. This report presents a review of speckle interferometry, including current status and results. Section 2 provides a background of the Fourier mathematics used in image processing and optical systems. Section 3 describes how the atmosphere degrades astronomical images and how speckle interferometry has been used to recover high-resolution detail. Section 4 describes new work to recover actual optics-limited images, and compares active optics systems with speckle interferometry.		

DD FORM 1 JAN 73 1473

Unclassified

SECURITY CLASSIFICATION OF THIS PAGE (When Data Entered)

82 11 30 049

AD A121940

DTIC FILE COPY

DTIC  
ELECTE  
NOV 30 1982

**AFGL-TR-82-0341**

**REPORT SD-TR-82-45**

①

**The AFGL Image Reconstruction Program II  
Speckle Interferometry**

**SIMON P. WORDEN, Capt., USAF  
Air Force Geophysics Laboratory  
and  
Department of Astronomy, University of California, Los Angeles**

**E. K. HEGE, E. N. HUBBARD, N. J. WOOLF  
and P. A. STRITTMATTER  
Steward Observatory, The University of Arizona**

**1 December 1981**

**Final Report**


**APPROVED FOR PUBLIC RELEASE;  
DISTRIBUTION UNLIMITED**

**SPACE DIVISION  
AIR FORCE SYSTEMS COMMAND  
Los Angeles Air Force Station  
P.O. Box 92960, Worldway Postal Center  
Los Angeles, Calif. 90009**

This report has been reviewed by the Public Affairs Office (PAS) and is releasable to the National Technical Information Service (NTIS). At NTIS, it will be available to the general public, including foreign nationals.

This technical report has been reviewed and is approved for publication. Publication of this report does not constitute Air Force approval of the report's findings or conclusions. It is published only for the exchange and stimulation of ideas.

FOR THE COMMANDER

  
Thomas W. Flattery, Col, USAF  
Program Manager  
Defense Dissemination Program



Accession For	
NTIS GRA&I	<input checked="checked" type="checkbox"/>
DTIC TAB	<input type="checkbox"/>
Unannounced	<input type="checkbox"/>
Justification	
By	
Distribution/	
Availability Codes	
Dist	Avail and/or Special
A	

## CONTENTS

I.	INTRODUCTION.....	1
II.	MATHEMATICAL BACKGROUND.....	7
	A. Fourier Mathematics.....	7
	B. The Fourier Transform: A Way of Representing Data.....	7
	C. Sampling Theorem.....	11
	D. Noise and Filtering.....	12
III.	OPTICAL SYSTEMS, IMAGE DEGRADATION, AND SPECKLE INTERFEROMETRY.....	17
	A. The Modulation Transfer Function.....	17
	B. The Effects of the Atmosphere.....	22
	C. Speckle Interferometry.....	23
	D. Isoplanicity.....	27
	E. Instrumentation for Speckle Interferometry.....	21
	F. Data Reduction.....	32
IV.	IMAGE RECONSTRUCTION.....	39
	A. Post-Processing Methods.....	39
	B. Wavefront Reconstruction Methods.....	48
V.	SUMMARY.....	55
	REFERENCES.....	57

## FIGURES

1.	Speckle Images (3 arc-second area) Taken on the Kitt Peak 4-Meter Reflecting Telescope.....	4
2.	Auto-correlation of a Function $f(x')$ .....	10
3.	Elimination of Noise in Power Spectra.....	13
4.	Diagram of Light Formation from a Small Element $ds$ of An Aperture .....	18
5.	Light Formation in an Optical Aperture.....	21
6.	Calculated Modulation Transfer Functions for Three Cases.....	24
7.	Schematic Representations of Image Formation.....	25
8.	Representation of Isoplanatic Angle.....	28
9.	Schematic Diagram of the Kitt Peak Photographic Speckle Camera Used by Lynds <u>et al.</u> (1976).....	29
10.	Laser Reduction of Speckle Photographs.....	33
11.	Optically (Laser) Produced Power Spectra of Two Binary Star Speckle Patterns.....	35
12.	Auto-correlation of a Binary Star Showing the Two Bright Maxima at Binary Separation.....	36
13.	Reconstructed Images and One-Dimensional Profiles for Alpha Orionis (Resolved Supergiant) and Gamma Orionis (Point Source) from Lynds <u>et al</u> (1975).....	41
14.	Solar Image with Portion Reconstructed Using the Knox-Thompson Algorithm.....	44
15.	Successful Reconstruction of a Binary Star (Alpha Auriga) and a Resolved Supergiant (Alpha Orionis) Using Phase Unwrapping Technique and Fienup Algorithm.....	45
16.	Two Types of Active Optical Systems.....	49
17.	Results of ITEK Rubber Mirror Test on Point Source Stars.....	51
18.	Operation of Hartman Active Optics System.....	53

## I. INTRODUCTION

In this document, we provide a tutorial and status report on methods for recovering image information degraded by turbulence in the Earth's atmosphere. This turbulence reduces angular resolution to about one arc-second, although theoretical limits of large optical telescopes are set by the telescope primary optics diameter. For typical circular apertures, this limit is given by the well-known Dawes' criterion:

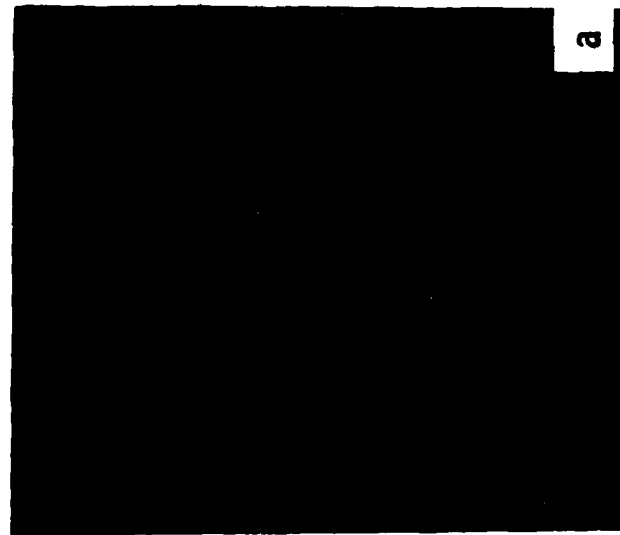
$$\Delta\theta = 2.1 \times 10^5 \frac{\lambda(\text{cm})}{d(\text{cm})} \text{ arc second} \quad (1)$$

where  $\lambda$  is the optical light wavelength and  $D$  the telescope diameter in centimeters. This formula predicts about 0.02 arc second resolution for large telescopes like the Hale 5-meter, a factor of 50 better than the atmospheric "seeing" limit. Although Michelson (1921) first succeeded in using a form of interferometry to reach the theoretical resolution limit for observations of astronomical objects, it was not until Labeyrie's (1970) hallmark work that real progress was made.

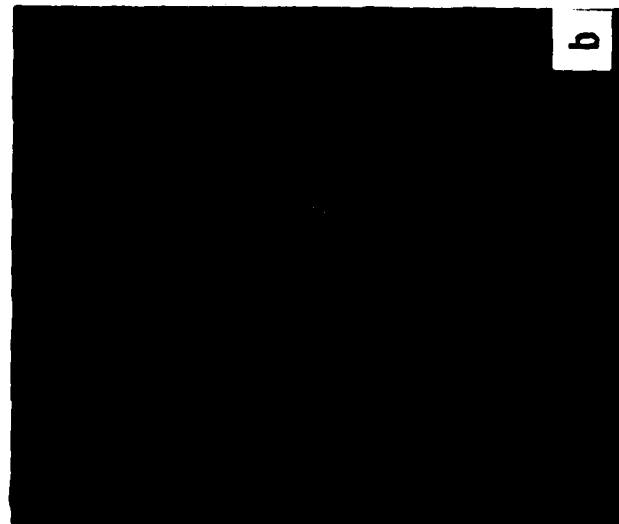
Labeyrie (1970) pointed out that a short exposure photograph of a star image contains identifiable and extractable information on angular scales approaching the Dawes limit given in Eq. (1). An example of short exposure star photos, at very large image scale, is given in Figure 1. The overall size of these images is about 2 arc-seconds. However, the small-scale structure within each image has a scale very close to the theoretical telescope diffraction limit. The character of this small-scale structure is noticeably different for the three stars; a point source, resolved supergiant star, and a close binary. These images are basically multiple-aperture interference patterns. The process of extracting high resolution results from these interference pattern images is therefore called "speckle interferometry."

The basic objective of speckle interferometry is to obtain the images on time scales short enough, typically 10 ms, so as to effectively freeze the turbulence in the Earth's atmosphere. It is these turbulence cells which,

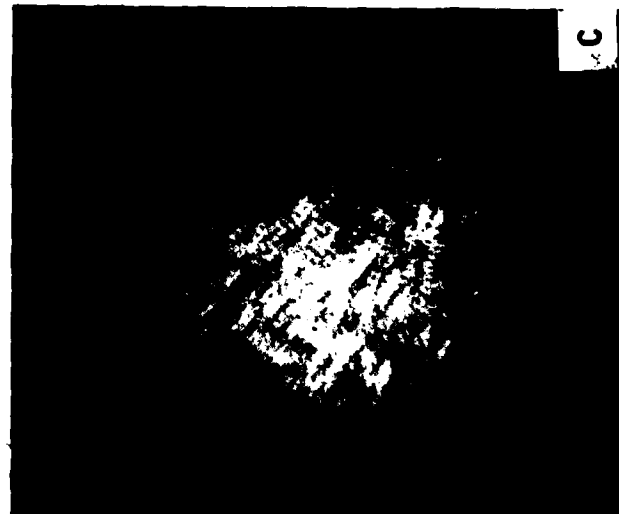




a



b



c

NOTE: a - Alpha Orionis, a resolved supergiant star with an angular diameter of 0.05 arc-second  
b - Gamma Orionis, a point source star  
c - Alpha Auriga, a binary star with an angular separation of 0.06 arc-second

Fig. 1. Speckle Images (3 arc-second area) Taken on the Kitt Peak 4-Meter Reflecting Telescope

through small temperature differences and corresponding index of refraction changes, break up the phase coherence of an incoming plane wave. A conventional long exposure photograph averages signals with rapidly varying wavefront errors. The resulting image has a resolution set by the average scale of coherence in the atmospherically broken up wavefront rather than the full telescope aperture. This scale is typically 10 cm, so that long-exposure photos have resolutions appropriate to only a 10-centimeter telescope, namely one arc-second. However, in speckle photos, the turbulence is frozen and the ensemble of small 10 cm coherence phase errors acts as a form of multiple aperture interferometer to yield information on the full diffraction-limited scale of the entire telescope. Speckle data was first reduced (Gezari et al., 1972) by optically computing the average power spectrum (Fourier amplitude) of many speckle photos. As will be discussed later in this paper, such results yield telescope diffraction-limited size and shape information.

For more detailed information, interested readers are directed to review articles by Dainty (1976), Worden (1977), and Labeyrie (1978). However, classical power spectrum analysis (Labeyrie 1978) does not provide sufficient information to reconstruct a full diffraction-limited image. Since 1970, an improved understanding of atmospherically induced image degradation has been reached and is described in these review papers. Two approaches, active optics and passive reconstruction, based on extensions to speckle interferometry, have particular promise for complete image reconstruction. Active optics, spearheaded by the ITEK Corporation, provide real-time image compensation and reconstruction. Active optics methods will not be extensively discussed in this report. We will concentrate on passive, after-the-fact image reconstruction techniques, and in particular on speckle interferometry.

Since Labeyrie's introduction, speckle interferometry has been used to measure the angular sizes of bright stars (cf Gezari et al., 1973) and to determine the orbits of binary stars (cf McAlister, 1978). From the latter, astrophysically important masses for the binary components may be extracted. Until recently, the speckle technique has suffered from two key problems which limited its usefulness to bright objects. Photographic recording systems have limited speckle work to objects brighter than stellar magnitude +7, and the

data reduction techniques developed by Labeyrie and his collaborators provide only diffraction-limited Fourier amplitude information on an object being observed. Although the object size and general shape are derivable from the Fourier amplitudes alone as mentioned above, the much more interesting diffraction-limited image requires the Fourier phases as well. These problems have been effectively addressed through support from the Air Force Geophysics Laboratory (AFGL) and Air Force Office of Scientific Research (AFOSR). We believe it is now possible to reconstruct actual images for objects as faint as stellar magnitude +15, encompassing many interesting astronomical targets as well as high-altitude, Earth-orbital satellites. In this report we provide a brief review of the relevant Fourier mathematics (Section II) followed by a discussion of current speckle interferometry techniques and hardware (Section III), with special attention to the newly developed University of Arizona speckle system. We conclude with a discussion in Section IV of currently available methods for recovering a complete diffraction-limited image, rather than merely size and shape.

## II. MATHEMATICAL BACKGROUND

### A. FOURIER MATHEMATICS

In this section we review the Fourier transform with special attention given to the auto- and cross-correlation functions. We provide a brief description of methods used in digital (computer) Fourier analysis. We then discuss how to properly sample data so as to preserve all available information and to understand the role of noise in real data. Finally, we review the image formation process in a typical optical system. Interested readers are referred to Bracewell's (1965,1978) book The Fourier Transform and Its Applications, for an extensive review of the necessary mathematical background. It is the primary reference for all that follows in Sections IIB and IIC.

### B. THE FOURIER TRANSFORM: A WAY OF REPRESENTING DATA

Data may be represented as a set of "intensities",  $f(x)$ , where  $f(x)$  is usually real and a function of a spatial coordinate "x". For physical data,  $f(x)$  is real and usually known only at a set of discrete locations, the measurement points. The consequences of this sampling are discussed in C below. There are a number of useful alternate representations of data. Fourier analysis is a way to decompose the intensity as a function of  $x$  into a series of sine and cosine curves.

$$f(x) = \frac{a_0}{2} + \sum (a_s \cos sx + b_s \sin sx) \quad (2)$$

This function is the Fourier series representation of data. The series representation is a periodic function which repeats itself outside some range of  $x$ . This representation is general and applies to complex functions as well as to real functions.

The exponential representation of sines and cosines is useful for ease in computation and notation. Following the definition

$$e^{ix} = \cos x + i \sin x \quad (3)$$

the substitution

$$\begin{aligned} \cos x &= \frac{e^{ix} + e^{-ix}}{2} \\ \sin x &= \frac{e^{ix} - e^{-ix}}{2i} \end{aligned} \quad (4)$$

eliminates the sine and cosine in the Fourier series Eq. (2) yielding

$$\begin{aligned} f(x) &= \frac{a_0}{2} + \sum \left( \frac{a_s - ib_s}{2} e^{isx} + \frac{a_s + ib_s}{2} e^{-isx} \right) \\ &= \sum_{s=-\infty}^{\infty} c_s e^{isx} \end{aligned} \quad (5)$$

where  $c_s$  is in general complex, even for real data, except for functions symmetric around zero. For integrable functions continuous on  $x$ , the coefficients in Eq. (5) are given by

$$c_s = \frac{1}{2\pi} \int_{-\infty}^{\infty} f(x) e^{-isx} dx = F(s) \quad (6)$$

which is the Fourier transform of  $f(x)$ , usually denoted by  $F(s)$ . For ease in showing the behavior of the complex  $F(s)$ , the square of the modulus of  $F(s)$ , more generally known as the "power spectrum" of  $f(x)$ ,

$$|F(s)|^2 = \sqrt{\text{Real}^2[F(s)] + \text{Im}^2[F(s)]} \quad (7)$$

is computed. Physical measurements involve the "convolution" of the desired quantity  $f(x)$  with the instrumental measurement profile  $g(x)$ . The convolution is defined as

$$o(x) = \int f(x') \cdot g(x - x') dx' \quad (8)$$

For ease in notation, convolutions are usually denoted by an asterisk

$$o(x) = f(x) * g(x) \quad (9)$$

This function has the interesting property that under the Fourier transform convolutions become multiplications

$$O(s) = F(s) \cdot G(s) \quad (10)$$

If the instrumental response function  $g(x)$  is known, and  $o(x)$  is observed, then the Fourier transforms  $G(s)$  and  $O(s)$  can be computed. The desired function  $f(x)$  can then be recovered by dividing  $O(s)$  by  $G(s)$  and inverting the transform.

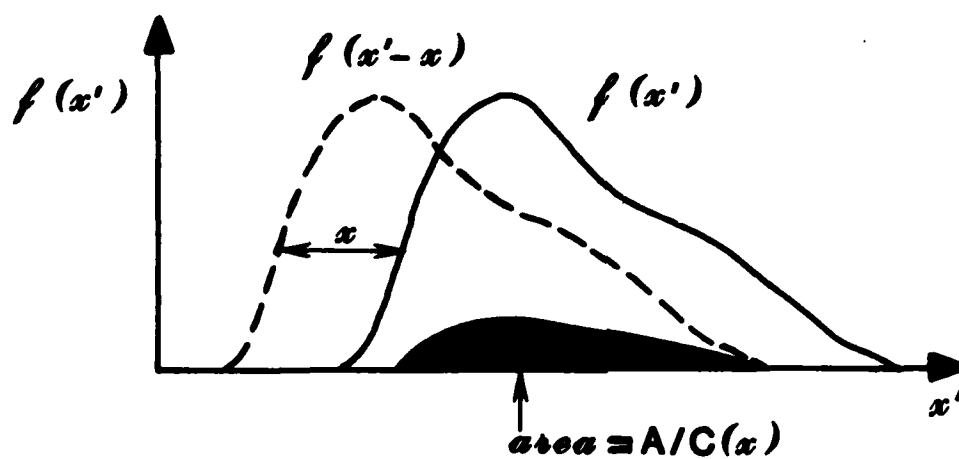
The "auto-correlation" is another useful function, which we will refer to as  $A/C(x)$ . The auto-correlation is constructed by convolving a function with itself, as opposed to the "self-convolution" in which the function is convolved with its reverse. The auto-correlation process is shown schematically in Figure 2.

$$A/C(x) = \int f(x') \cdot f(x' - x) dx' \quad (11)$$

This is a function useful for revealing mean scales and periods in a data set. A useful aspect of auto-correlations is stated in the auto-correlation theorem: "The auto-correlation is the Fourier transform of the power spectrum."

$$A/C(x) = \int_{-\infty}^{\infty} |F(s)|^2 e^{-i\pi s x} ds \quad (12)$$

Another useful aspect of Fourier analysis is that the zero frequency or DC component of the Fourier transform  $F(0)$  is always real and represents the area (or average) under the curve  $f(x)$  for the limits of the Fourier integration or summation.



NOTE: Auto-correlation of a function  $f(x')$  at a given value of  $x$  is the multiplication of  $f(x')$  with  $f(x' - x)$  represented by the shaded area.

Fig. 2. Auto-correlation of a Function  $f(x')$

For data sets,  $f(x)$ , sampled only at the picture elements (pixels) labeled  $x$ , discrete Fourier transforms over the set of pixels  $x = \{x_1, x_2 \dots x_N\}$

$$F(s) = \sum_{x_1}^{x_N} f(x) e^{-i2\pi xs} \quad (13)$$

may be computed. A direct calculation of this sum for each Fourier frequency  $s$  can be time-consuming on even a large computer. However, this calculation is made simple by use of the Fast Fourier Transform algorithm (FFT) which reduces the computations required for  $n$  points so that the overall speed is proportional to  $N \log_2 N$ , rather than  $N^2$  as might be expected from the fact that there are as many Fourier frequencies  $s$  as data pixels  $x$ . Programs are especially fast for arrays with an even power of 2 elements.

### C. SAMPLING THEOREM

It is important to consider how best to sample a continuous function. This question is addressed in the "Sampling Theorem" below, and it has special importance for processing data. Physical data generally varies in a well-behaved manner (e.g., bounded and continuous). We therefore expect that we could sample the data at some evenly spaced interval and not lose any information. The sampling theorem provides the requirements for this and states:

IF A FUNCTION IS 'BAND-LIMITED' (HAS A NON-ZERO FOURIER TRANSFORM FOR FREQUENCIES  $s < s_c$  AND A ZERO TRANSFORM FOR  $s > s_c$ , WHERE  $s_c$  IS REFERRED TO AS THE 'CRITICAL' FREQUENCY OR NYQUIST FREQUENCY), THEN THE FUNCTION IS FULLY SPECIFIED BY VALUES SPACED AT EQUAL INTERVALS NOT EXCEEDING  $1/2 s_c^{-1}$  SAVE FOR ANY HARMONIC TERM WITH ZEROS AT THE SAMPLING POINTS.

An example of such a function is the Airy disc of a diffraction-limited telescope aperture. In this case, the critical frequency is the classic Dawe's criterion limit in Eq. (1). Thus, if we have a diffraction-limited image, we should sample the image at twice the diffraction limit.



#### D. NOISE AND FILTERING

Many astronomical noise sources have well defined transforms which may be partially separated and removed from the desired "data" transform. Equation (10) may be used to recover and restore results degraded by a smearing function by a simple inversion. If one observes a function  $o(x)$  and knows the instrumental response function  $g(x)$ , then the transform of the true function  $f(x)$  is the Fourier deconvolution.

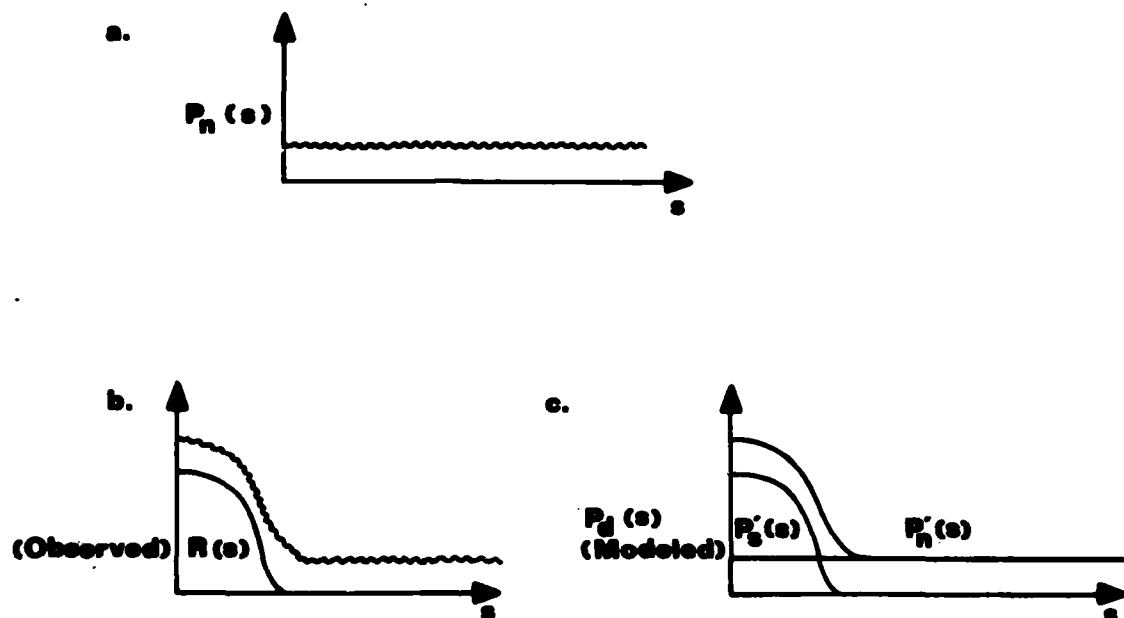
$$F(s) = O(s) \cdot G(s)^{-1} \quad (14)$$

Noise is always present in real data. The observed function  $o(x)$  contains both a real signal  $s(x)$  and a noise component  $n(x)$ . For simplicity, the noise is assumed to be additive, random, and uncorrelated with the signal as shown in Figure 3a.

$$o(x) = s(x) + n(x) \quad (15)$$

If one naively restores  $o(x)$  using Eq. (14), the high frequency noise is strongly enhanced and will totally dominate the results. For critically sampled data, the highest frequency components typically contain at least as much noise as signal. Typical restoring functions (instrumental response corrections) enhance high frequencies proportionately more than low frequencies. The restored function thus has noise enhanced as much or more than signal. It is therefore desirable to find a restoring function which would correct the data to as close as possible to the true function, and at the same time, suppress rather than enhance high-frequency noise components. An optimum restoring function is the Wiener filter (cf Wiener, 1949). Brault and White (1971) provide an excellent summary of methods for Wiener filtering astronomical data.

Following Brault and White (1971), Wiener filtering produces the best estimate,  $R(s)$  shown in Figure 3b, of the true function Fourier Transform  $F(s)$ . The optimum weighting of the frequency components in the deconvolution



NOTE: In "a" we see the "white" or constant power spectrum of typical noise. In practice, we observe in "b" the addition of noise signal and a real signal  $R(s)$ . To account for noise effects, we model in "c" the total signal  $P_d(s)$  consisting of both the modeled real signal  $P'_s(s)$  and the estimated noise signal  $P'_n(s)$ . With these models, Brault and White (1971) show that optimum noise removal and restoration for degrading functions is possible.

Fig. 3. Elimination of Noise in Power Spectra

$$R(s) = \frac{O(s)}{G(s)} \Phi(s) \quad (16)$$

is the optimum filter  $\Phi(s)$ . This Wiener filter is derived as described in Brault and White (1971) and it takes the form

$$\Phi(s) = \frac{P_s(s)}{P_s(s) + P_N(s)} \quad (17)$$

where  $P(s)$  is the power spectrum of the degraded signal

$$\begin{aligned} P_s(s) &= |F(s) \cdot G(s)|^2 \\ &= |S(s)|^2 \end{aligned} \quad (18)$$

and  $P_N(s)$  is the power spectrum of the noise

$$P_N(s) = |N(s)|^2 \quad (19)$$

The actual calculation of  $\Phi(s)$  as represented in Eq. (17) is difficult since it involves both the quantity  $S(s)$  which we are trying to measure and the interfering noise  $N(s)$ . Since  $\Phi(s)$  is an optimum filter in the least squares sense, small deviations from the true filter shape give only second order error increases. In practice, the complicated signal and noise power spectra are replaced by the simplified smooth models shown in Figure 3c. The observed signal,  $O(s)$ , is also modeled with a smooth curve,  $P_d(s)$ . As specified above,  $P_d(s)$  is the sum of the signal model  $P'_s(s)$  and noise model  $P'_N(s)$

$$P_d(s) = P'_s(s) + P'_N(s) \quad (20)$$

$P'_s(s)$  and  $P'_N(s)$  replace  $P_s(s)$  and  $P_N(s)$  in Eq. (17). For most astronomical data the noise is assumed to be "white," with no systematic frequency dependence. For example, white noise is characteristic of random statistical fluctuations in photon flux measurements. For most stellar images, a gaussian is a good estimate of the stellar image profile characteristics

$$P'_s(s) = C_1 e^{-\left(\frac{s}{C_2}\right)^2} \quad (21)$$

$$P'_N(s) = C_3 \quad (22)$$

where the constants  $C_1$ ,  $C_2$ , and  $C_3$  are chosen to best represent the observed results.

### III. OPTICAL SYSTEMS, IMAGE DEGRADATION, AND SPECKLE INTERFEROMETRY

#### A. THE MODULATION TRANSFER FUNCTION

To determine the character of an image formed by an optical telescope, we begin with a discussion of an electromagnetic antenna following Bracewell (1965). Although the discussion is one-dimensional, it can easily be generalized to two dimensions. We proceed from Figure 4 with light propagating from left to right. At each point in the aperture plane, the instantaneous electric field in the propagating light wave is given by  $F(s) \cos [wt - \phi(s)]$  where  $w$  is the angular frequency of the monochromatic light. The propagating wave is thus generalized in time by a complex "phasor,"  $\vec{E}(s)$ , with an amplitude  $F(s)$  and a phase  $\phi(s)$

$$\vec{E}(s) = F(s) e^{-i\phi(s)} \quad (23)$$

To deduce the configuration of the light at a distant "image" plane, Huyghens' principle is applied. That is, the complex phasor at a distant point will be the sum of the effects gotten by propagating the phasor from each element in the aperture plane. At some point  $P$  in the image plane at a distance  $R$  from the origin ( $s = 0, z = 0$ ) consider the effects of a small element in the aperture plane,  $ds$ , at a distance  $r$  from  $P$ . The infinitesimal element  $ds$  produces an effect at  $P$  proportional to the amplitude  $F(s)$  at  $ds$ , but with the phase retarded by the number of cycles contained in the path  $r$  from  $ds$  to  $P$ . Thus, the element between  $s$  and  $s + ds$  produces at  $P$

$$\begin{aligned} d\vec{E}(P) &= F(s) e^{-i\phi(s)} ds e^{-i2\pi r/\lambda} \\ &= \vec{E}(s) ds e^{-i2\pi r/\lambda} \end{aligned} \quad (24)$$

where  $\lambda$  is the monochromatic wavelength. To simplify the problem, we specify  $r$  in terms the distance of  $P$  from the origin  $R$ . If  $R$  makes an angle  $\theta$  with the  $z$  axis, then for small angles:

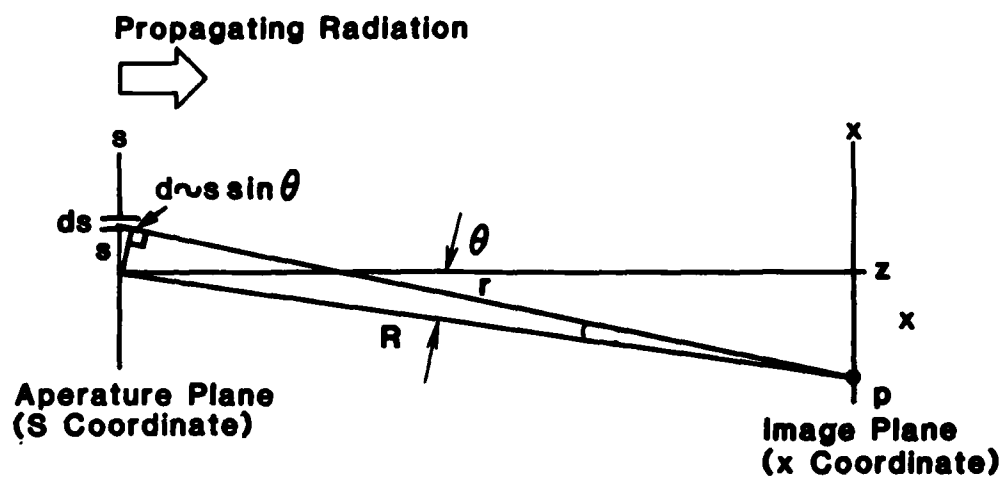


Fig. 4. Diagram of Light Formation from a Small Element  $ds$  of an Aperture

$$\begin{aligned}
 r &= R + d \\
 &\approx R + s \sin \theta
 \end{aligned}
 \tag{25}$$

We specify the coordinate in the image plane in angular units, again with the small angle approximation

$$\begin{aligned}
 x &\equiv \theta \\
 &\approx \sin \theta
 \end{aligned}
 \tag{26}$$

Equation (24) now becomes, substituting  $x$  for  $\sin \theta$  in Eq. (25)

$$d\vec{E}(P) = \vec{E}(s) e^{-i2\pi sx/\lambda} ds$$

To determine the effects of all points in the aperture, we integrate over  $ds$ :

$$\begin{aligned}
 \vec{O}(x) &= \int_{-\infty}^{\infty} d\vec{E}(p) ds \\
 &= \int_{-\infty}^{\infty} \vec{E}(s) e^{-i2\pi R/\lambda} e^{-i2\pi sx/\lambda} ds
 \end{aligned}
 \tag{27}$$

The factor  $e^{-i2\pi R/\lambda}$  expresses the average phase retardation from all aperture elements and is a complex proportionality constant  $C$  which we will not consider further.

$$O(x) = C \int_{-\infty}^{\infty} \vec{E}(s) e^{-i2\pi sx} ds \tag{28}$$

From the definition in Eq. (6), we see that the "image" at a plane distant from the aperture is related to the aperture distribution through the Fourier transform. For an optical system such as a telescope, with light propagating on axis from a distant source, the focal plane is the angular transform of the aperture plane as described above. In this instance,  $\vec{O}(x)$  is known as the Optical Transfer Function, or OTF. Therefore, to determine the angular light wave properties in a telescope image plane, one computes the Fourier Transform of the aperture function  $\vec{E}(s)$ .

As an example of an image formation calculation for a simple aperture function, we consider a rectangular aperture with constant phase and amplitude across the aperture as displayed in Figure 5a. This "rectangle" function, of unit height and width, is denoted in standard optical terminology as the " $\Pi$ " symbol. Normalizing the units to wavelength, we have

$$\begin{aligned} \vec{O}(x) &= \int_{-\infty}^{\infty} \vec{E}\left(\frac{s}{\lambda}\right) e^{-i2\pi\left(\frac{s}{\lambda}\right)x} \frac{ds}{\lambda} \\ &= \int_{-\infty}^{\infty} \Pi\left(\frac{s/\lambda}{w}\right) e^{i2\pi\frac{s}{\lambda}x} \frac{ds}{\lambda} \\ &= w \frac{\sin wx}{wx} \\ &= w \operatorname{sinc}\left(\frac{wx}{\pi}\right) \end{aligned} \quad (29)$$

with the width of the aperture,  $w$ , in units of wavelength. This sinc function result is the familiar function displayed in Figure 5b.

The measureable quantity, light intensity, is the squared modulus of the OTF. Light from a distant point source will arrive at the telescope aperture in a form very similar to the model described above, with constant phase and amplitude across the aperture. The resulting point source image intensity function, the squared modulus of the OTF, is known as the Point Spread Function, or PSF (Figure 5c).

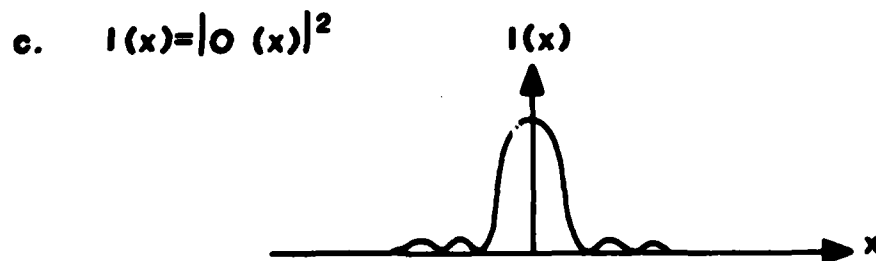
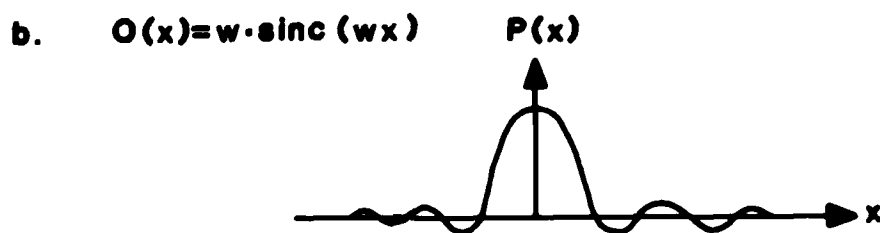
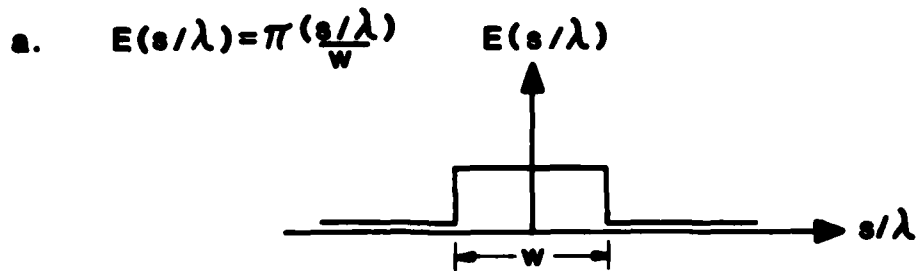
$$I(x) = |O(x)|^2 \quad (30)$$

To determine what the observed image,  $j(x)$ , would look like as compared to the "real" image,  $k(x)$ , one simply convolves  $k(x)$  with PSF

$$j(x) = k(x) * I(x) \quad (31)$$

The PSF  $\{I(x)\}$  generally includes the degrading effects of the detector as well as the optical imaging system. Since convolutions become multiplications under the Fourier Transform, Eq. (31) is usually replaced with its transform for ease in analysis





NOTE: In "a," light is allowed to pass only in the rectangular aperture  $W$ . In "b," we see the Fourier Transfer, or Optical Transfer Function (OTF) for the rectangular aperture, in this case a simple sinc function. The image intensity is given by the OTF in "c" and is known as the Point Spread Function.

Fig. 5. Light Formation in an Optical Aperture

$$J(s) = K(s) \cdot i(s) \quad (32)$$

$i(s)$  is the Modulation Transfer Function or MTF. Often the MTF modulus or squared modulus  $(MTF)^2$  is displayed to confine the results to real numbers

$$\begin{aligned} MTF &= i(s) \\ &= \int_{-\infty}^{\infty} I(x) e^{-12\pi xs} dx \\ &= \int_{-\infty}^{\infty} |O(x)|^2 e^{-12\pi xs} dx \end{aligned}$$

Recalling the definition of  $O(s)$  given in Eq. (28) and that the auto-correlation function is the Fourier Transform of the power spectrum [Eq. (12)], it follows that the MTF is the auto correlation of the aperture function  $\vec{E}(s)$

$$MTF = \int_{-\infty}^{\infty} \vec{E}(s') \cdot \vec{E}(s' - s) ds' \quad (33)$$

#### B. THE EFFECTS OF THE ATMOSPHERE

For light transmitted through the atmosphere, the aperture function has two components

$$\vec{E}(s) = \vec{E}_0(s) \cdot \vec{A}(s) \quad (34)$$

where in one dimension,  $\vec{E}_0(s)$  is the standard rectangular (or in two dimensions, circular) pupil function  $\Pi(s)$ .  $\vec{A}(s)$  contains the contribution for propagation through the atmosphere and is in general complex and variable in both amplitude and phase. The amplitude variations are due to transmission variability of the atmosphere and the phase fluctuations caused by index of refraction variations. The refractive index variations are attributed to small-scale density inhomogeneities within the atmosphere. There are a variety of models for  $\vec{A}(s)$ , but a generally applicable one is the "log normal" model where the logarithms of the amplitude and phase variations are each

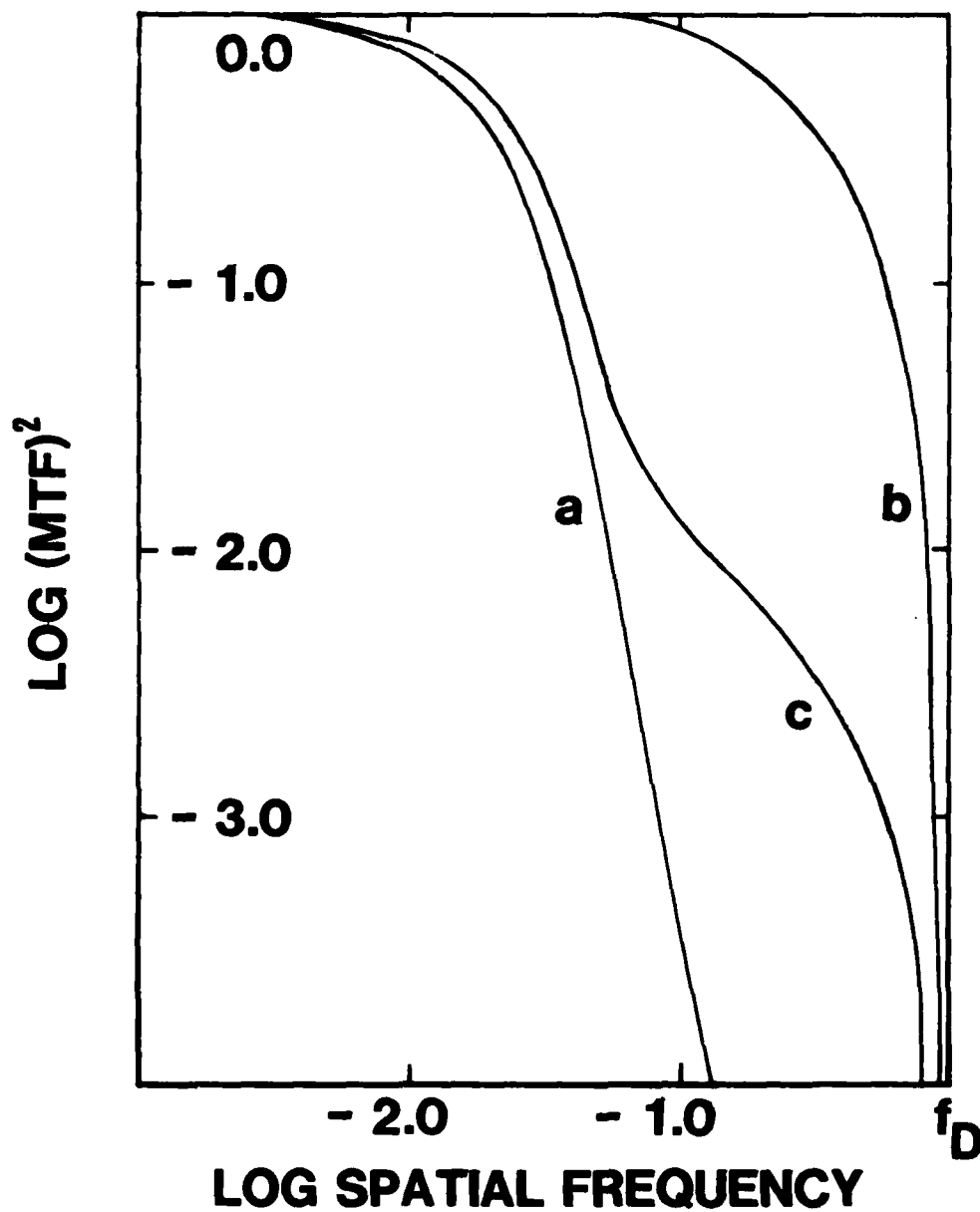
assumed to have gaussian distributions. The linear scale of the fluctuations obey a characteristic (Kolomogorov) spectrum with a mean scale of  $r_0$ , where  $r_0$  is typically of order 10 cm. Korff (1973) and Korff et al. (1972) have carried out the integration in Eq. (34) using log normal atmospheric models and have shown that in short-exposure photos where  $A(s)$  is instantaneously "frozen," the average  $MTF^2$  of many such photos (denoted by brackets) has two components

$$\langle MTF^2 \rangle = |\langle MTF \rangle|^2 + K \cdot MTF_{DIF} \quad (35)$$

where the first term on the right is the MTF averaged over long time periods and thus is the conventional long-exposure, degraded MTF with no signal at frequencies higher than the 1 arc-second atmospheric cutoff. The second term, however, is the undegraded diffraction-limited MTF appropriate to the full telescope aperture, but reduced by a factor  $K$ .  $K$  is typically of order  $r_0/D$ , where  $D$  is the telescope diameter. In Figure 6, we show the calculated MTF for long and short exposures as well as the diffraction-limited case. As stated previously, a conventional long-exposure photo has a MTF with no signal at high frequencies. However, short-exposure data does indeed contain frequency information out to the diffraction limit, albeit considerably reduced from the information in a photo obtained with no atmospheric effects; for example, from a space telescope.

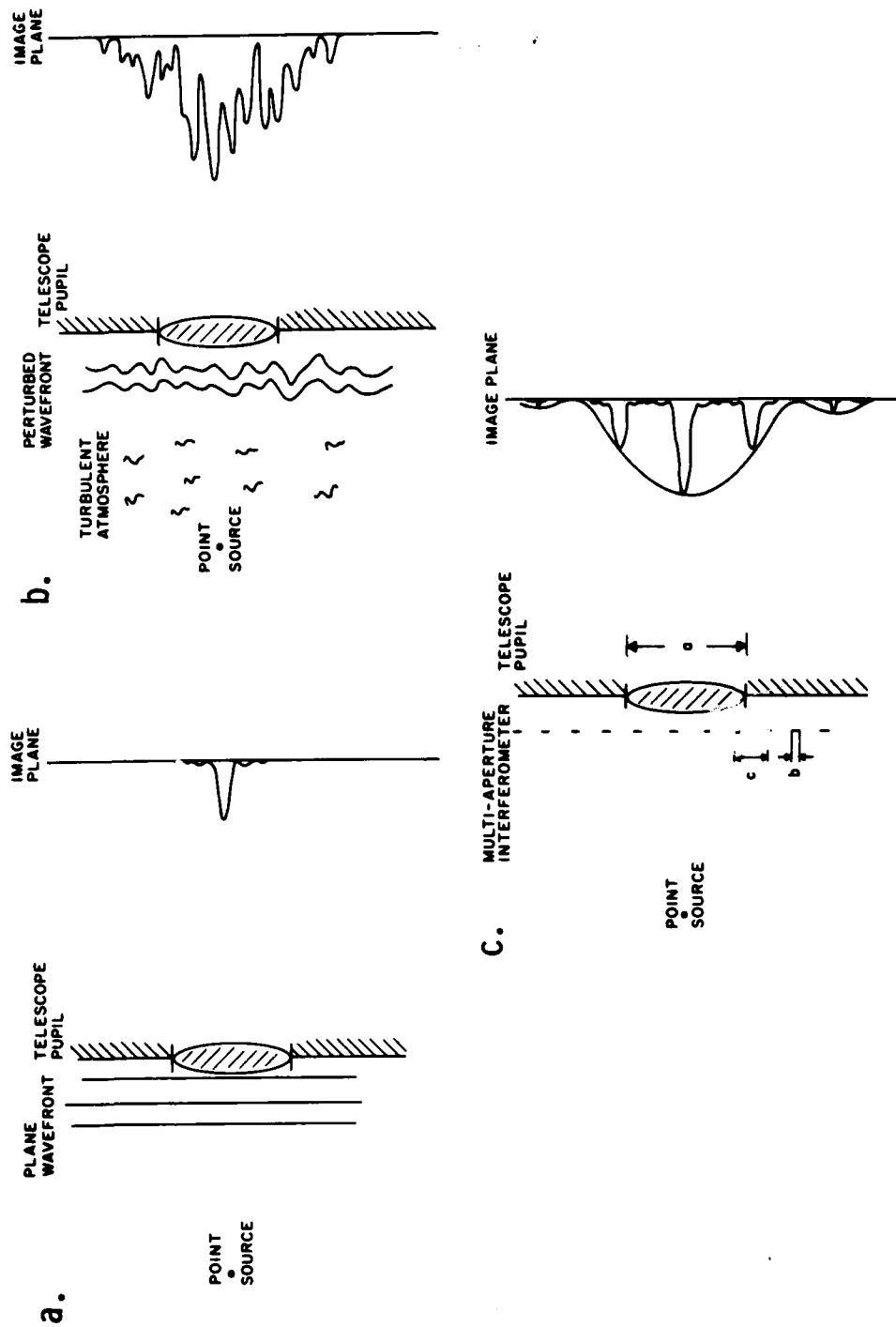
### C. SPECKLE INTERFEROMETRY

We will now review the detailed appearance of short-exposure astronomical photographs. Korff and his collaborators have carried through the calculations outlined above. His results show that short-exposure photos exhibit a two-dimensional interference or "fringe" pattern with the mean image scale of the fringes comparable to the telescope diffraction limit. These fringes are the "speckles" apparent in Figure 1. The same result can be derived using a considerably simpler model for the aperture function  $\vec{E}(s)$  than the log normal model. The short exposure process may be modeled as the multiple aperture interferometer shown in Figure 7. For undegraded images (Figure 7a), the aperture function is the constant rectangle function in Figure 5 and the



NOTE: a - Unperturbed (no atmospheric degradation) image  
 b - Degraded, long-exposure image  
 c - Speckle short-exposure photograph "c" has finite signal out to the theoretical undegraded limit, while the long-exposure data do not.

Fig. 6. Calculated Modulation Transfer Functions for Three Cases



NOTE: a - An unperturbed wave front  
 b - The short-term atmospheric case with 10 cm phase (and amplitude) errors across the telescope aperture  
 c - A multiple-aperture interferometer  
 Note that b and c both retain high frequency (resolution) structure.

Fig. 7. Schematic Representations of Image Formation

resultant image becomes the well-known  $\text{sinc}^2$  function discussed in Section IIIA. In two dimensions, this process produces the classic Airy disk. But the real case in 7b, computed by Korff, is somewhat similar to the multiple aperture interferometer in Figure 7c if we restrict ourselves to only one phase. For random atmospheric fluctuations, the individual apertures of size  $b \approx r_0$  are more or less evenly distributed across an aperture of diameter =  $a$ , with spacing between sub-apertures =  $c$ , the aperture function can be written

$$E(s) \approx \Pi\left(\frac{s}{a}\right) \cdot \text{III}\left(\frac{s}{c}\right) * \Pi\left(\frac{s}{b}\right) \quad (36)$$

In this conceptual oversimplification, the first term is a rectangle function appropriate to the full aperture. The second and third terms represent a Dirac comb denoted in optical parlance by the "shah" symbol,  $\text{III}\left(\frac{s}{c}\right)$  (representing a set of impulses) distributing by convolution the small apertures of size  $b$ ,  $\left[\Pi\left(\frac{s}{b}\right)\right]$ , across the whole aperture at spacing  $c$ . Since convolutions become multiplications under a transform and rectangle functions  $\text{sinc}$  functions, it follows from Eq. (29) that the image intensity is:

$$\begin{aligned} I(x) &= |O(x)|^2 \\ &= \text{sinc}^2(ax) * \text{III}^2(cx) \cdot \text{sinc}^2(bx) \cdot \text{constant} \end{aligned} \quad (37)$$

The first term is the full undegraded telescope diffraction spot, distributed by a new Dirac comb impulse set  $\text{III}(cx)$ . The third term is a diffraction spot appropriate to a much smaller aperture of size  $b = r_0$ . This broad spot modulates and clips our array of narrow, high resolution spots. For  $r_0 = 10$  cm, this latter function is about 1 arc-second wide, or more simply, the diffraction-limited spot of a 10 cm telescope! The model assertion that short-exposure speckle images consist of a set of displaced diffraction limited images modulated by a 1 arc-second seeing disk, is supported by the photos shown in Figure 1. The individual "speckles" in 1a are double for a binary and those for the resolved star in 1c larger than the point source in 1b. In work discussed later, Lynds et al. (1976) showed that the individual

speckle profiles for a point source do indeed closely resemble telescope diffraction-limited Airy disks.

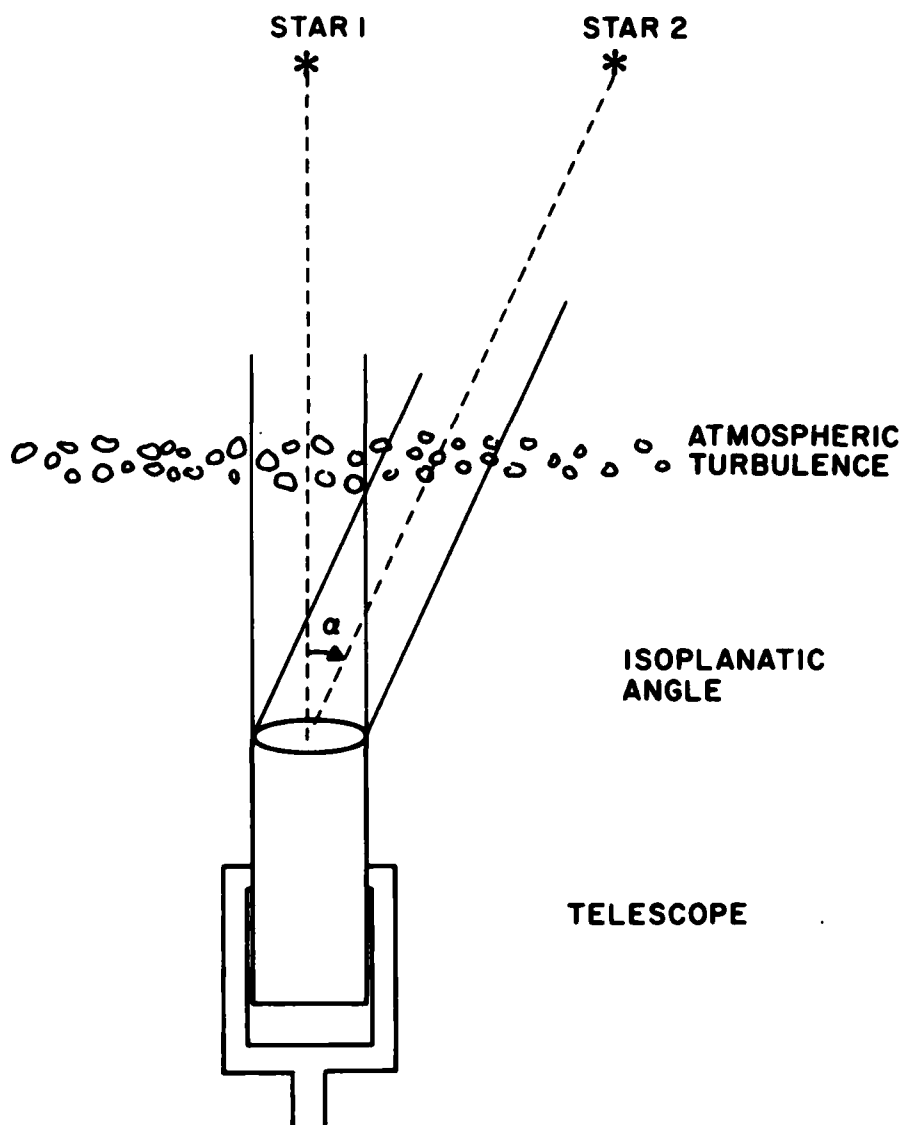
#### D. ISOPLANICITY

Atmospheric image degradation has one further complication which we will now discuss. This is the isoplanatic limitation shown diagrammatically in Figure 8. Light from one point source outside the atmosphere does not travel through the same column of turbulent atmosphere as light from another nearby point source. Depending on the angular distance between the two sources and the height within the atmosphere where the incoming plane waves are broken up, the instantaneous degradation may not be identical. The maximum angle where the perturbations are correlated is known as the isoplanatic angle. No rigorous definition of this angle is generally accepted. For our purposes, we have defined it as the angle where the cross-correlation between the individual speckle patterns of the components of a binary star system fall to  $1/e$  of their maximum possible (auto-correlation) value. Using this definition, Hubbard et al. (1979) have measured the isoplanatic angle to lie between 4 and 7 arc-seconds depending on physical conditions and star position on the sky. There is some evidence (Hardy 1979) that the isoplanatic angle may be as small as one arc-second for daytime seeing conditions. Despite the many uncertainties, the effective isoplanatic angle is probably never greater than 10 arc-seconds, although there are some assertions in the literature to the contrary (Weigelt, 1979) but these are not substantiated by a quantitative criterion such as the one we have proposed.

#### E. INSTRUMENTATION FOR SPECKLE INTERFEROMETRY

In this section we will review the basic features of speckle data acquisition systems. In Figure 9, we show a diagram of Lynds et al. photographic system. Starting from the left, the device consists of:

1. A fast shutter to insure exposures shorter than the atmospheric change time, typically 20 ms.
2. A set of rotating prisms (Risley prisms) are set to counteract atmospheric dispersion. Since the desired results are diffraction limited, we must consider errors on scales of a few thousandths of an arc-second. The atmosphere acts like a prism for objects away



NOTE: Isoplanatic angle is the angle over which light from two sources passes through the same turbulent atmosphere.

Fig. 8. Representation of Isoplanatic Angle



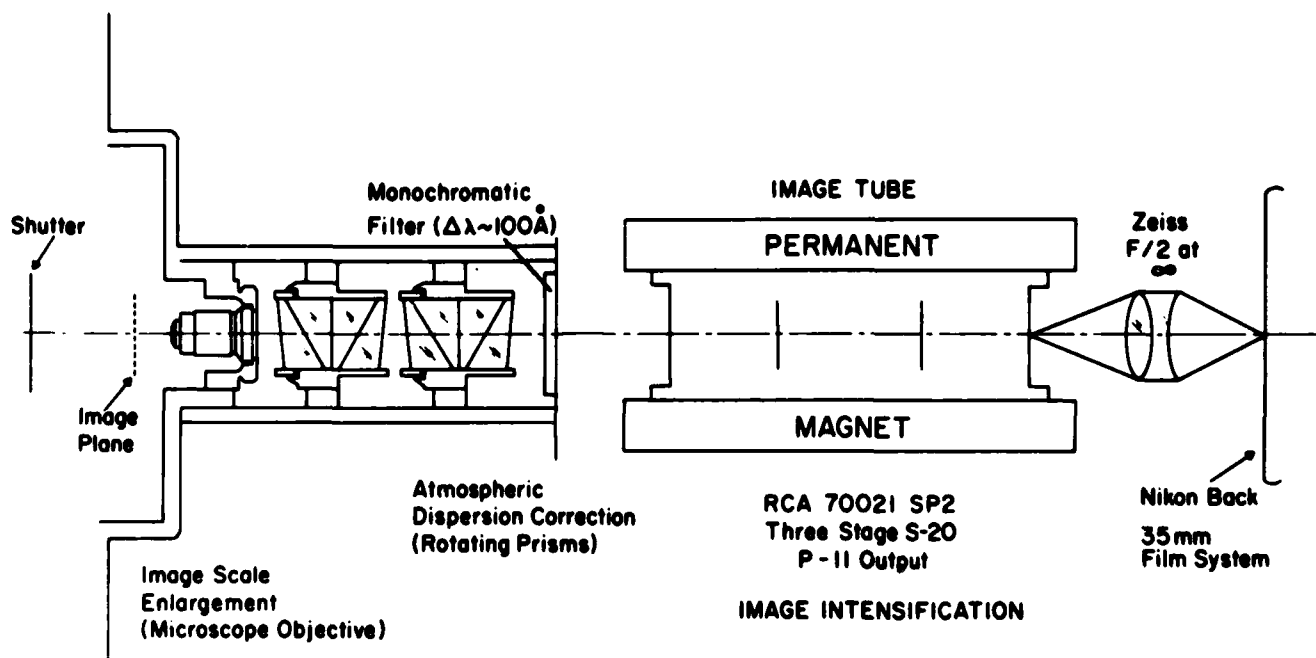


Fig. 9. Schematic Diagram of the Kitt Peak Photographic Speckle Camera Used by Lynds et al. (1976)

from the zenith. At the small angular scales we are dealing with, this effect can substantially smear the speckle pattern for even very narrow bandpasses of a few hundred Angstroms.

3. A microscope objective or similar optics expands the image scale so that typical detectors, film in this case, critically oversample (sampling theorem) the telescope diffraction-limited spot. For the 4-meter telescope the final image scale is 0.2"/mm, in which case the telescope diffraction spot of ".03 represent 150  $\mu$ , an easily sampled size for film or digital detectors.
4. An interference filter defines the spectral bandpass. Since there may be up to 30 orders of interference across a large telescope speckle pattern, the bandpass must be less than about  $\lambda/30$  or 150 Å. Naturally, larger telescopes produce speckle patterns with more orders of interference, thus requiring narrower bandpasses.
5. To provide enough signal so that individual photon arrivals may be rapidly detected on film (or other detectors) image intensification is used. For most systems, a three-stage, magnetically focused image tube appropriately coupled to the detector is ideal.
6. For simple systems, as shown here, the speckle frames are recorded photographically using a commercial 35 mm, single lens reflex camera with motorized film transport. The low efficiency and frame rates plus the cumbersome data reduction for film systems have limited photographic systems to objects brighter than magnitude +7. It is the final detection and recording area where substantial gains may be achieved with modern digital detectors.

The photographic system outlined can in principle detect individual photons if the image intensification is large, but this presents substantial difficulties. The usual photographic features such as film grain and development artifacts can easily be misidentified as photons. Image tube noise such as ion events present a similar problem. Faint objects produce only a small bandpass speckle photo, so the large two-dimensional data recording ability of film is wasted. Of most concern is the requirement for up to  $10^6$  speckle frames digitally processed for satisfactory results on faint object data. If current photographic digitization schemes are used, about 5 minutes is required to digitize one frame! Afterglow in the image tube requires that the shutter be cycled only once per second so that the tube returns to a dark condition between exposures. This process wastes most of the photons since only one 20-ms exposure is obtained per second. To obtain

$10^6$  exposures with such a system would require weeks, and to process them would require years. Steward Observatory has developed a digital system to eliminate these problems (Hege et al., 1980). The instrument is similar to that developed at the University College, London (cf Boksenberg, 1978).

In the University of Arizona instrument, the output of the image tube is recorded continuously on video tape without shuttering the speckle camera. All possible data is thus recorded at television rates (60 cycles/sec). A video analog-to-digital unit constructed by Grinnell Systems converts the video tape into computer-compatible numbers and inputs each frame into an associated array processor which identifies, centers, and thresholds the photons to determine each photon location and discriminate against large ion events and low level noise. To eliminate false identifications of photons based on the afterglow of a photon arrival from a previous frame, each frame is differenced against its immediate predecessor to insure that only new photon arrivals are identified. The resulting photon coordinates alone may then be recorded onto digital tape or input into an array processing computer for immediate auto-correlation or Fourier transform calculations. The procedure may be run in real time so the whole process is done at the telescope. We have refined Boksenberg's system by recognizing that 6-9 pixels are necessary to oversample each telescope diffraction spot. The Boksenberg system only oversamples by the standard Nyquist factor of 2-3 and we have found empirically that this does not provide sufficiently accurate photon coordinates to reach the full telescope diffraction limit. These procedures are described in Strittmatter (1980).

Other systems exist for identifying and recording individual photons. An especially novel system has been developed by L. Mertz at Lockheed which sequentially identifies photon arrivals, rather than recording all events within a given exposure. Mertz (1979) has developed a method for completely reconstructing images which requires knowledge of when a photon arrives vis-a-vis other photons rather than just where it arrives.

#### F. DATA REDUCTION

Labeyrie's method for processing speckle photons stems directly from the standard image reconstruction deconvolution equation

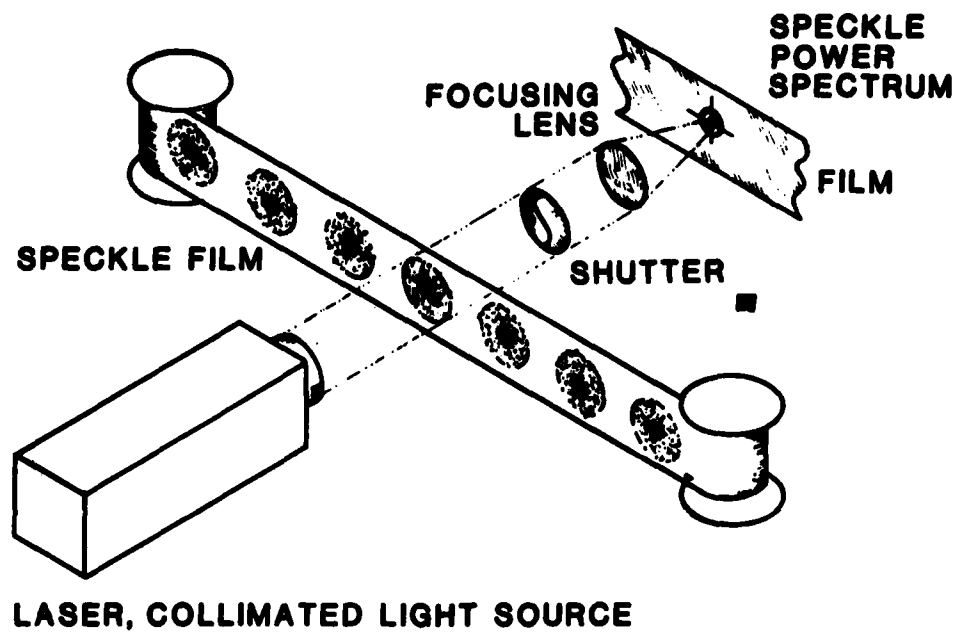
$$K(s) = \frac{J(s)}{i(s)} \quad (38)$$

where  $K(s)$ ,  $J(s)$ ,  $i(s)$  are respectively the noise-corrected Fourier transforms of the desired image  $k(x)$ , the observed image  $j(x)$ , and the point spread function  $I(x)$ . To reiterate, this equation does not work to recover full diffraction-limited images from conventional long-exposure photos. The Modulation Transfer Function  $i(s)$ , usually obtained from observations of point source stars, contains no high-frequency information in a long-exposure regime. The deconvolution in Eq. (25) shows that short-exposure data does contain a finite MTF out to the telescope diffraction limit. This desired signal is, however, only extractable in a statistical sense. In Eq. (25), Labeyrie's contribution was to note that the mean squared modulus from many speckle frames contains a finite and presumably constant diffraction-limited term. We can thus use the deconvolution in Eq. (27) to obtain the diffraction-limited power spectrum (squared modulus) of an object outside the atmosphere

$$|K(s)|^2 = \frac{\langle |J(s)|^2 \rangle}{\langle |i(s)|^2 \rangle} \quad (39)$$

where the top term is the average power spectrum of a set of target object speckle patterns and the bottom term the same function for a set of point source (star) speckle photos, both properly corrected for noise bias. To insure the assumption that average transfer properties of the point source and program object are identical, point source observations are generally made as closely as possible in time and location in the sky as those of the program object.

The power spectrum computations are done either optically or digitally. In the optical mode, a coherent light source (laser) is shone through the speckle film as shown in Figure 10. The light is then brought to a focus.



NOTE: Focused laser light which has passed through speckle photos produces a power spectrum of these photos.

Fig. 10. Laser Reduction of Speckle Photographs

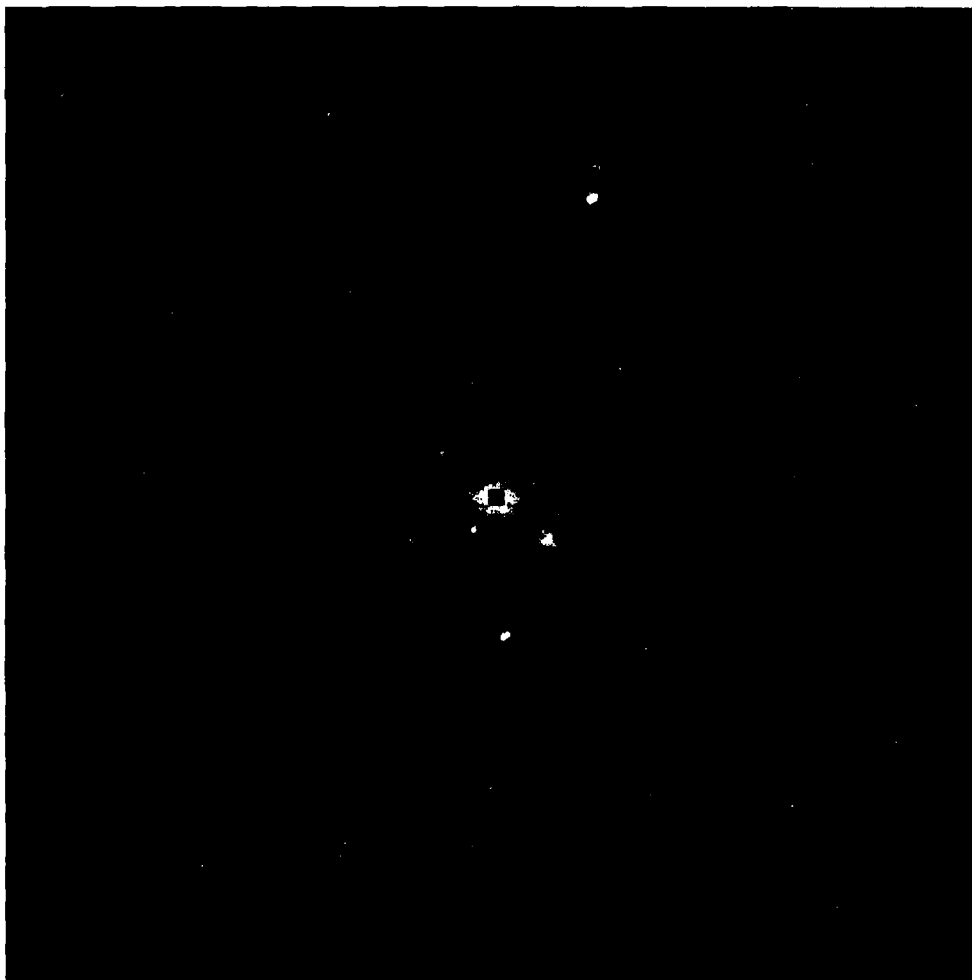
Following our earlier discussion, the focused product is a power spectrum. The signal from many speckle photos may be added to produce results such as those shown in Figure 11 for close binary stars. This method is well suited to binary stars since the binary power spectrum has the easily detectable banding apparent in Figure 11. Binary star angular separation and position angle are readily obtained from such data, often without need of point source comparison data. The binary star auto correlation is sometimes computed from the power spectrum since the binary signal is concentrated into two small points as shown in Figure 12 rather than the diffuse power spectrum bands. This makes it easier to extract results. The procedures outlined above may be done on a computer for digitized speckle data, thereby providing more careful control of the process. Since new speckle systems provide digital data, the optical reduction method has fallen into disuse. We remind the reader that only Fourier amplitudes are extracted with Labeyrie's method; the phase and complete image recovery are lost.

To derive angular diameters rather than relative separations, we need to measure the precise point where the diffraction-limited power spectrum cuts off. This is more difficult than measuring the position of bands in binary star power spectra. The diameter signal is overlaid on a background of noise and atmospheric interference. Speckle results are generally calibrated from the point source observations, which stresses the assumption that the point source has identical transfer characteristics and no noise bias. Even a small difference between the point source and target object transfer characteristics can obscure angular size determinations. To account for this problem, Worden et al. (1977) derived a method to calibrate directly from the target object results, without reference to an external point source. The method involves computing the mean auto-correlation between speckle frames of the same set of data. The cross-correlations must be between exposures far enough apart in time, typically 1 second, so that all diffraction-limited signal is gone, as it is the cross-correlation which provides the calibration. Moreover, the program object must be smaller than the atmospheric 1 arc-second cutoff. Welter and Worden (1979) have shown that this process, represented in Eq. (41), produces a full diffraction-limited auto-correlation, undegraded by



**NOTE:** The closely separated fringes are for Beta Cepheus with a binary separation of 0.25 arc-seconds. The more widely separated fringes are from Iota Serpentis with a binary separation of 0.1 arc-second.

**Fig. 11. Optically (Laser) Produced Power Spectra of Two Binary Star Speckle Patterns**



NOTE: May be computed from the Fourier Transform of data shown in Fig. 11

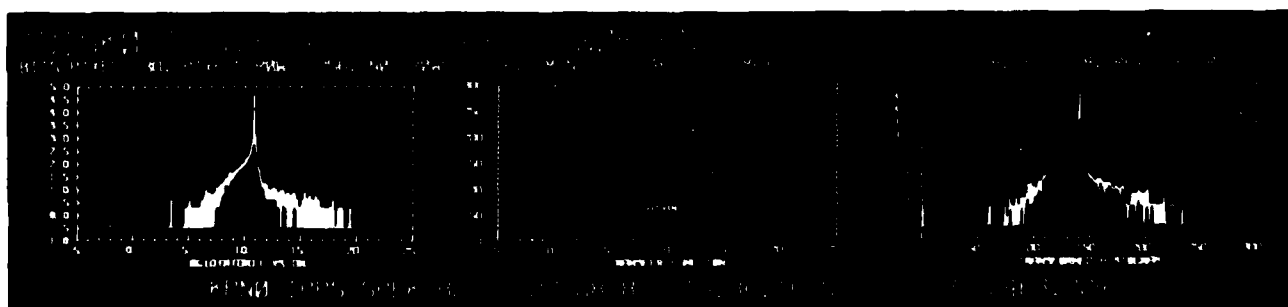


Fig. 12. Auto-correlation of a Binary Star Showing the Two Bright Maxima at Binary Separation



atmospheric effects. Hege et al. (1980) have shown that the appropriate cross-correlation function may be much more readily calculated from a single long-exposure image accumulated from the same set of exposures.

$$k(x) * k(x) = j_1(x) * j_1(x) - c * j_1(x) * j_{1+1}(x) \quad (40)$$

The constant  $c$  has been shown by Hege et al. (1980) to be necessary to normalize the results. It is the constant which makes the cross-correlation identical to the auto-correlation at sizes much larger than the object but smaller than the 1 arc-second cutoff. Moreover, each speckle frame must be carefully centered and normalized before processing, otherwise, the cross-correlation will have a spread not present in the auto-correlation, giving systematic errors (Worden and Stein, 1979). This method is ideal for faint object speckle data since the correlations and long-exposure images are easy to compute from photon locations. The correlations are simply the vector distance between photon locations and may be computed in real time at the telescope.

We make an additional point concerning the handling of noise in speckle images. For virtually all stellar speckle applications, the raw speckle data consist entirely of individual photon locations, as described previously. The auto-correlations of this signal and associated noise provide an additional source of interference in extracting quantitative results. In an ideal sense, photon noise should be confined to a single pixel. In practice, however, detectors are seldom good enough that random noise is confined to a single pixel. In either case, it is essential to account for this noise "bias" in a consistent manner. It is generally desirable to oversample the telescope diffraction-limited scale by as large a factor as possible to separate the noise bias error from the diffraction-limited signal. However, practical considerations of detector size limit the degree to which oversampling is possible. Clearly, in any speckle system the noise bias will have real impact at the spatial frequencies where diffraction-limited signal is desired.

The Arizona speckle reduction process handles the noise bias in the following manner. For ease in notation, we consider the power spectra of

photon sampled speckle frames, with  $N_1$  photons in each frame. Following Eq. (12), the net observed power spectrum  $P_{OBS}(s)$  is computed from the transform of the auto-correlation in Eq. (41).

$$P_{OBS}(s) = 1/2\pi \int |k(x) * k(x)|^2 e^{-12\pi xs} ds \quad (41)$$

The noise bias power spectrum,  $P_{ph}(s)$ , is obtained by collecting many frames of faint uniform illumination (no stellar signal) integrations and computing the average power spectrum of these frames, normalized to a single photon. The observed power spectrum is then divided by this bias power spectrum. To normalize the final result for a quantitative estimate of the true power spectrum,  $P_{EST}(s)$ , the total number of photons observed,  $N = \sum_1 N_1$ , is subtracted as a constant from the result. This is the crucially important noise bias correction

$$P_{EST}(s) = \frac{P_{OBS}(s)}{P_{ph}(s)} - N \quad (42)$$

We have shown that this formalism provides the best estimate of the actual object power spectrum, independent of the detailed form of detector response to photon noise.

#### IV. IMAGE RECONSTRUCTION

##### A. POST-PROCESSING METHODS

The ultimate goal of speckle inteferometry is to provide actual images completely free from atmospheric degradation. Any image has a Fourier transform  $K(s)$  which in general consists of amplitudes  $A(s)$  and phases  $e^{\phi(s)}$ .

$$K(s) = A(s) e^{\phi(s)} \quad (43)$$

As previously described, speckle interferometry provides diffraction-limited Fourier amplitudes  $A(s)$ . Most speckle image reconstruction methods center around efforts to recover the phase  $e^{\phi(s)}$ , as well. In 1976, Lynds, Worden, and Harvey accomplished the first complete speckle image reconstruction for the special case of bright, nearly point source targets where images could be extracted directly from the speckle photo. Knox and Thompson (1974) proposed a method to derive phases in a statistical manner related to Labeyrie's method for getting the amplitudes. The Knox-Thompson method has been successfully applied to the sun (Stachnik et al., 1977) but is highly noise sensitive and to date has only been applied to bright objects like the solar surface. Recently, Fienup (1978) proposed a method to derive phases by iterative processing using only the diffraction-limited amplitudes and some reasonable physical constraints on real physical image properties as inputs. This method is less sensitive to noise and we believe it is well suited for all image reconstruction work. It should provide actual images for all objects towards which speckle interferometry is applicable down to stellar magnitude +16 or fainter. We also note that active optics systems show considerable promise for bright object imagery.

Liu and Lohman (1973) and Wang (1974) pointed out that if a point source lies within the isoplanatic patch of a target object, the speckle pattern of the point source may be used as the instantaneous PSF. In this case, Eq. (38) may be used for direct Fourier deconvolution using only a single speckle frame. Unfortunately, there are precious few objects with a bright point

source within their isoplanatic patches. Weigelt (1978) has proposed to use a number of point sources sharing "partial isoplanicity" (i.e. within 10-20 arc-seconds) to perform the deconvolution. This method looks promising, but is still only applicable for a limited class of targets in bright fields of point sources.

As described previously, the speckles themselves can be thought of as images. This follows directly from the simple multiple aperture interferometric model for speckle interferometry. Repeating the result in Eq. (38):

$$I(s) = \text{sinc}^2(ax) * III(cx) \cdot \text{sinc}^2(bx) \cdot \text{constant} \quad (44)$$

The resulting image will consist of a set of impulses convolved with a diffraction-limited image and modulated by a seeing disk. Although actual speckle photographs are not true multiple aperture interferograms and individual "speckles" true Airy disks, it is apparent in Figure 1 that the speckles have a characteristic shape and size similar to an Airy disk as theoretically suggested by Korff et al. (1972). Since the speckle pattern of an object consists of the convolution of the actual object with a point source speckle pattern, individual speckles within such speckle patterns may be considered as the convolution of point source speckles with the object. Lynds et al. (1976) made use of this feature to reconstruct images of the resolved supergiant star Alpha Orionis (Betelgeuse). For binary stars, faint objects, or larger resolved objects it becomes difficult to pick out individual speckles since they overlap. The problem may be alleviated somewhat by restricting oneself to only the brightest speckles which are more widely separated within the speckle image. In practice, digital speckle photographs are computer-processed to locate and co-add bright speckles. Resulting "images" for Alpha Orionis and an unresolved comparison star are shown in Figure 13, along with our one-dimensional radial averages of these results. The similarity of the point source profile to an Airy disk, complete with secondary maxima, supports the simple multiple aperture model and validity of the technique. Refinements to this procedure have been proposed by Bates et al. (1978).

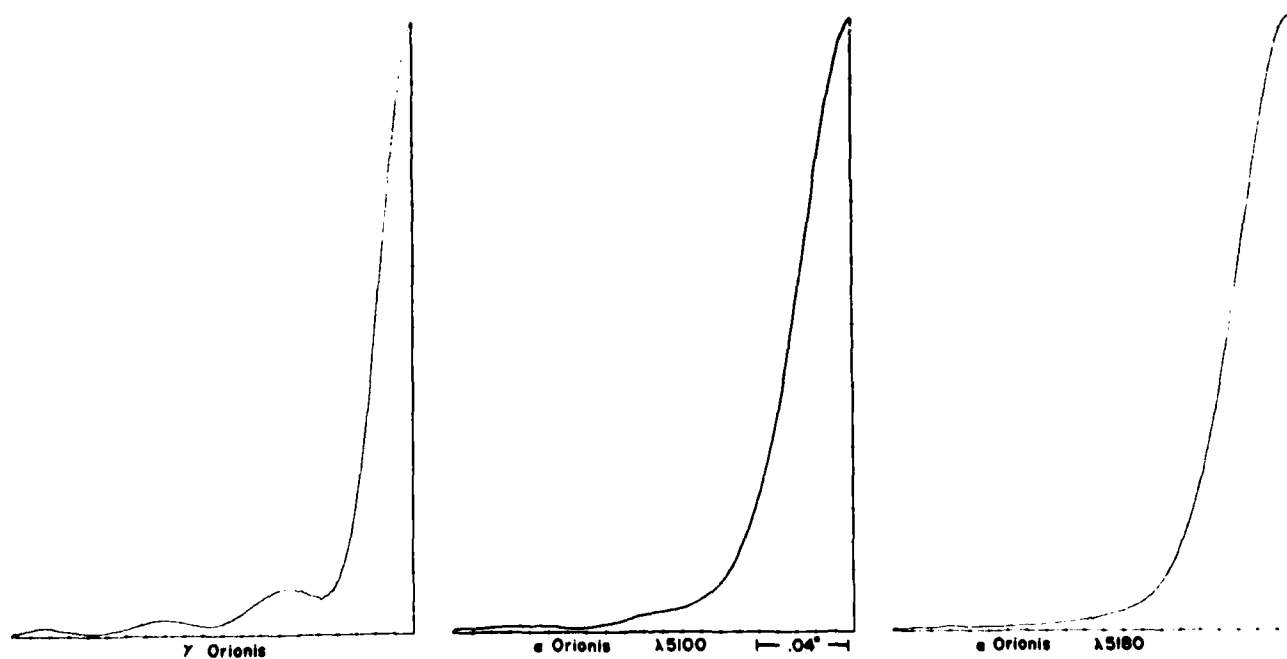
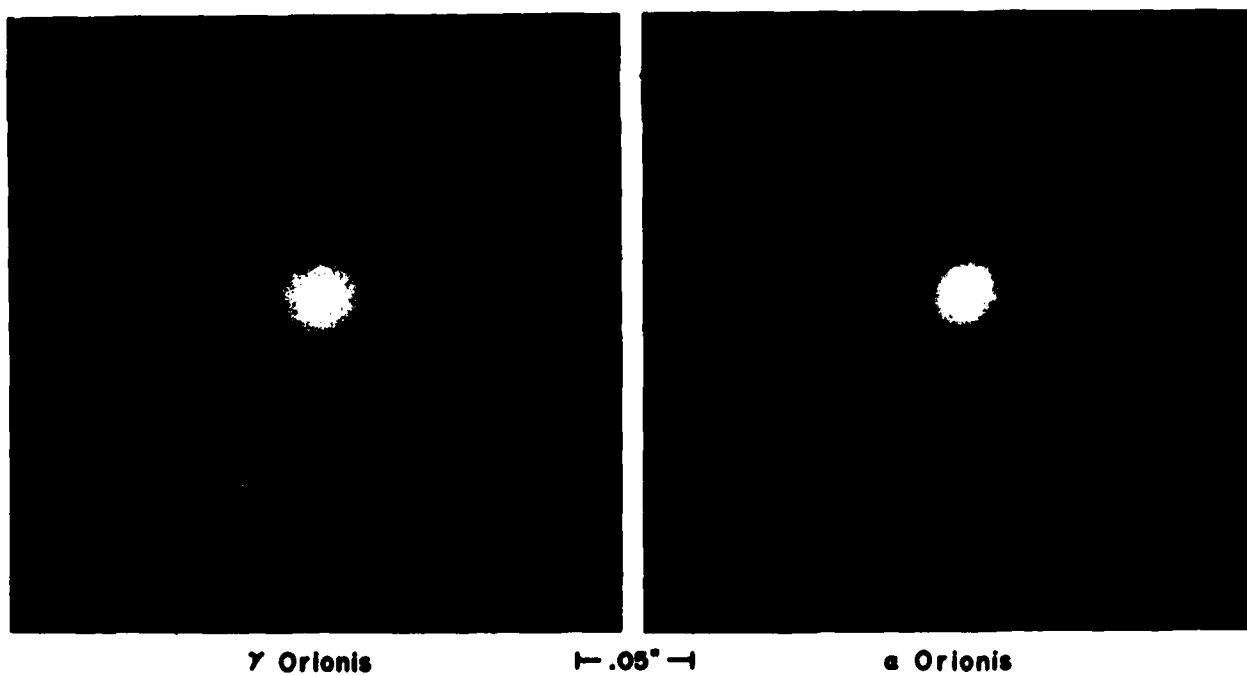


Fig. 13. Reconstructed Images and One-Dimensional Profiles for Alpha Orionis (Resolved Supergiant) and Gamma Orionis (Point Source) from Lynds et al. (1975)

A general-purpose image reconstruction scheme for arbitrarily shaped objects has been proposed by Knox and Thompson (1974) and Knox (1975). As previously discussed, the amplitude of the image Fourier transform can be obtained from Labeyrie's reduction technique. However, a similar averaging scheme involving the instantaneous phase was shown to fail by Miller et al. (1973) and McGlamery (1971). If the Fourier transforms of speckle frames are averaged, the result is identical to a conventional long-exposure photograph. The reason for this lies in the fact that at high spatial frequencies, the atmosphere introduces phase shifts large compared to  $2\pi$ . Since phase is periodic over  $2\pi$ , averaging phase with many cycles error results in zero values for both phase and amplitude. However, Knox and Thompson (1974) pointed out that the phase difference between nearby frequency points in speckle transforms undergoes atmospherically induced errors which are small compared to  $2\pi$ . The true value of phase difference between nearby frequencies may thus be obtained by averaging the instantaneous phase difference from each in a set of speckle photos. As with Labeyrie's method for obtaining amplitudes, phase differences systematically introduced by the telescope and detector are obtained from sets of calibration point source speckle data. To get the actual phase of each frequency element, this array of phase differences is processed via a simple algorithm. The DC or zero frequency element always has zero phase. The calculated phase differences may then be used to offset from zero to the actual phases for adjacent frequency elements. The process is then continued to higher frequencies using the already calculated lower frequency phases as new baselines. It is easy to see that small errors will propagate and worsen as one works out to higher frequency elements. Even though this error can be lessened somewhat by using multiple routes in frequency space for each frequency element (Stachnik et al., 1977) or by phase unwrapping techniques (Cocke, 1980), it is clear that the method is highly noise sensitive. Phase unwrapping techniques entail adding an additional requirement to speckle data reduction; that phases from one frequency element to adjacent frequencies vary in a smooth and continuous manner. Processing data with this additional constraint has yet to be fully investigated, but preliminary results (Cocke, 1980) suggest an improved performance in the presence of noise in the input data.

Stachnick et al. (1977) demonstrated the Knox-Thompson method for solar images producing the results in Figure 14. The sun is an ideal target for this method since low noise data is readily available, and the sensitivity of this method is minimized. Recently, the Harvard group (Nisensen, Stachnik, and Noyes, 1980) have succeeded in reconstructing a large area of the solar surface using the Knox-Thompson method. This approach thus shows great promise for solar physics work.

Until recently, the ability to reconstruct images of faint objects appeared to be beyond reach. The novel approach to this problem recently proposed by Fienup (1978) proceeds from work by Gerchberg and Saxton (1972) which showed that the Fourier phases could be derived in some cases solely from Fourier amplitude information. Fienup's method uses an iterative process operating in image space (i.e., not in transform space as the Knox-Thompson method) but using the Fourier amplitudes, which are readily extractable from conventional speckle methods, as inputs. We have successfully applied this method to a variety of objects, including the binary star shown in Figure 15, and we believe it completes the speckle method and accomplishes the ultimate goal of completely removing atmospheric degradation of images.

Fienup's algorithm is elegantly simple and proceeds as follows:

1. We know the "real" Fourier transform amplitude from speckle interferometry reduced in a manner described earlier.
2. We guess at an image. If no other information is available, an array of random numbers is a good start. If the object size is known, perhaps from the amplitudes in 1, the array of random numbers may be constrained to fit this size. Some residual phase information in the long-exposure image may also provide useful additional constraints.
3. Compute the Fourier transform of the image guess.
4. Force the computed transform amplitude of the guess to equal the known amplitude from 1. Do not touch the phases.
5. Invert the adjusted transform to recover an image.
6. Force the image in Step 5 to obey known image constraints, such as that there are no negative numbers, or that outside a certain size known from 1, all values are zero. This corrected image serves as the input for the next iteration.

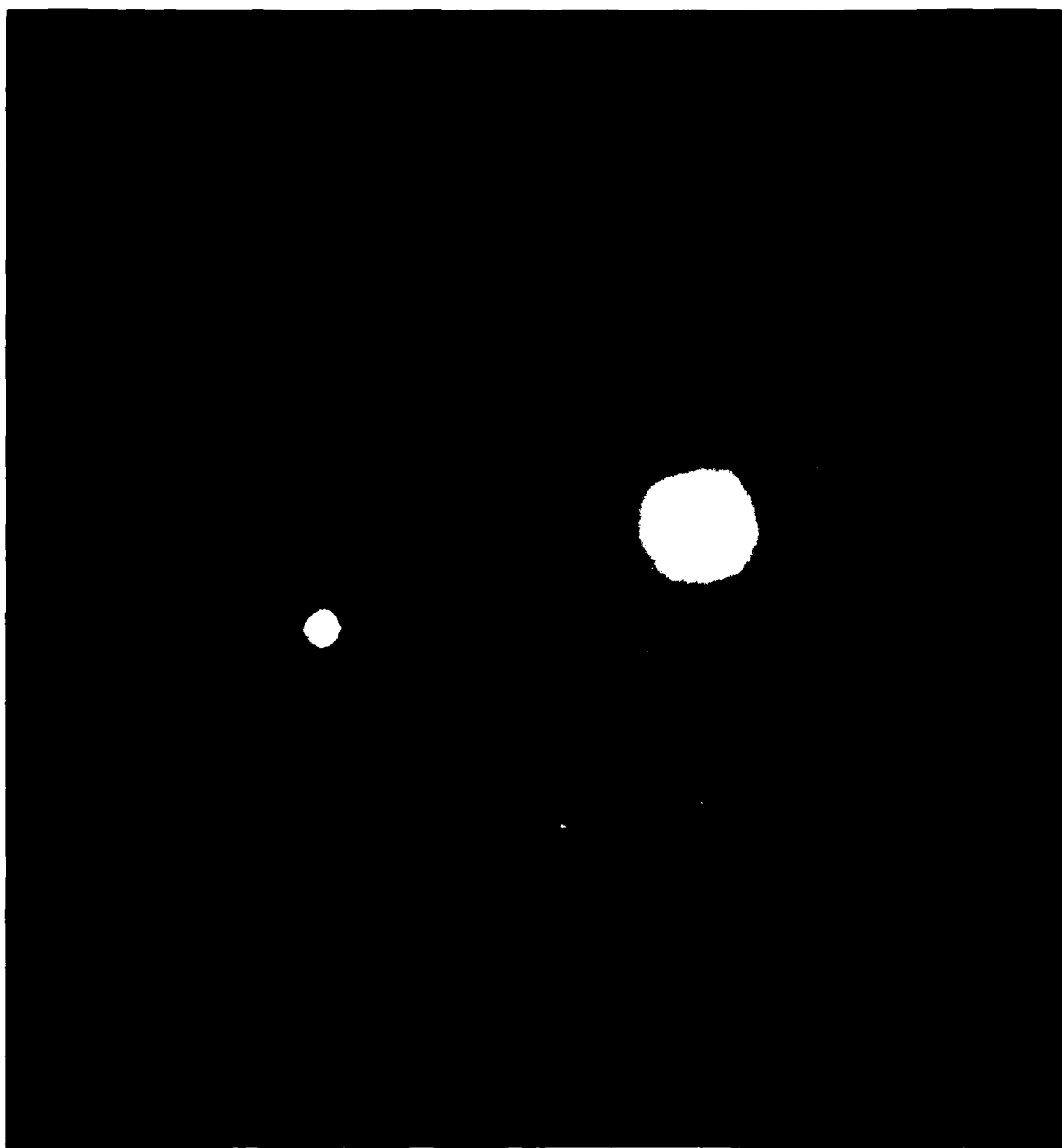


NOTE: Data from Stachnik et al. (1977)

0 2 4 6 8  
arc sec

Fig. 14. Solar Image with Portion Reconstructed Using the Knox-Thompson Algorithm





NOTE: Alpha Auriga - 0.050 arc-second separation  
Alpha Orionis - 0.06 arc-second angular diameter

Fig. 15. Successful Reconstruction of a Binary Star (Alpha Auriga) and a Resolved Supergiant (Alpha Orionis) Using Phase Unwrapping Technique and Fienup Algorithm

7. Iterate Steps 3-6 until a goodness-of-fit criterion is met such as the following given by Fienup:

$$E_o^2 = \frac{\iint \{j_i(s)\}^2 ds}{\int_{-\infty}^{\infty} \{j_i(s)\}^2 ds} \quad (45)$$

where  $j_i(s)$  is the  $i$ th image guess and the integral at the top is integrated over all locations  $\gamma$  where the constraints in 6 are not met.  $E_o$  will always decrease as explained by Fienup. Usually good images have  $E_o \lesssim 10^{-2}$ .

Since its publication, the uniqueness of solutions given by Fienup's (1978) method has been debated. Bruck and Sodin (1979) showed that the Fienup process does not give a unique result for one-dimensional functions. They also showed that for a two-dimensional image with an intensity function  $i(x,y)$ , the Fienup result is unique (plus or minus 180) unless  $i(x,y)$  is a factorable polynomial. If  $i(x,y)$  can be written as the product of two functions  $g(x,y)$  and  $h(x,y)$

$$i(x,y) = g(x,y) \cdot h(x,y) \quad (46)$$

where  $g(x,y)$  is a polynomial and  $h(x,y)$  is analytic everywhere without singularities except at infinity, then  $i(x,y)$  is factorable and the Fienup result is not unique. As discussed by Huizer and van Toorn (1980), this is a highly restrictive requirement for two-dimensional functions. They show a number of real two-dimensional functions which can be factored and have identical power spectra, but with greatly different forms. However, these functions are highly symmetric and do not resemble real space objects which are in general not factorable. On the other hand, Huizer and van Toorn (1980) pointed out that noise in the input data may make the polynomial factoring requirement considerably less restrictive, and thus Fienup reconstructions more ambiguous. Against this potential difficulty must be balanced successful evidence of the Fienup method such as shown in Figure 15 and more recent results such as given in Fienup's (1980) paper using our data. Both of these results were based on input data with substantial noise. Pending further study and simulations, the uniqueness of Fienup algorithm results must be regarded as an open issue.

We believe that an optimum procedure will combine phase retrieval methods such as Knox-Thompson, Cocke, or Bates to produce initial image estimates which will constrain the Fienup reconstruction sufficiently to remove image ambiguities even in the presence of substantial noise.

Our program, which retrieves the speckle phase information by both phase unwrapping and Knox-Thompson (K-T) methods, also computes the averaged power spectrum. This program works as follows: A digitized speckle frame is read from tape by the computer and Fourier transformed (FT). The squared modulus of this FT (the power spectrum) is added into the power spectrum accumulator array. Then, the phase angles of the FT are treated by the phase-unwrapping part of the program, which makes the phase angles as nearly continuous as possible, as a function of the discrete wave numbers (u,v). These unwrapped phase angles are added into the appropriate phase accumulator array. Also, the K-T phase-factor ratios are computed from the same FT and are added into another accumulator array.

The next speckle frame is read from the tape and processed as above, and so on until the desired number of frames N has been processed. The accumulator arrays are then divided by N, the result being the averaged power spectrum, unwrapped phase angles, and K-T ratios.

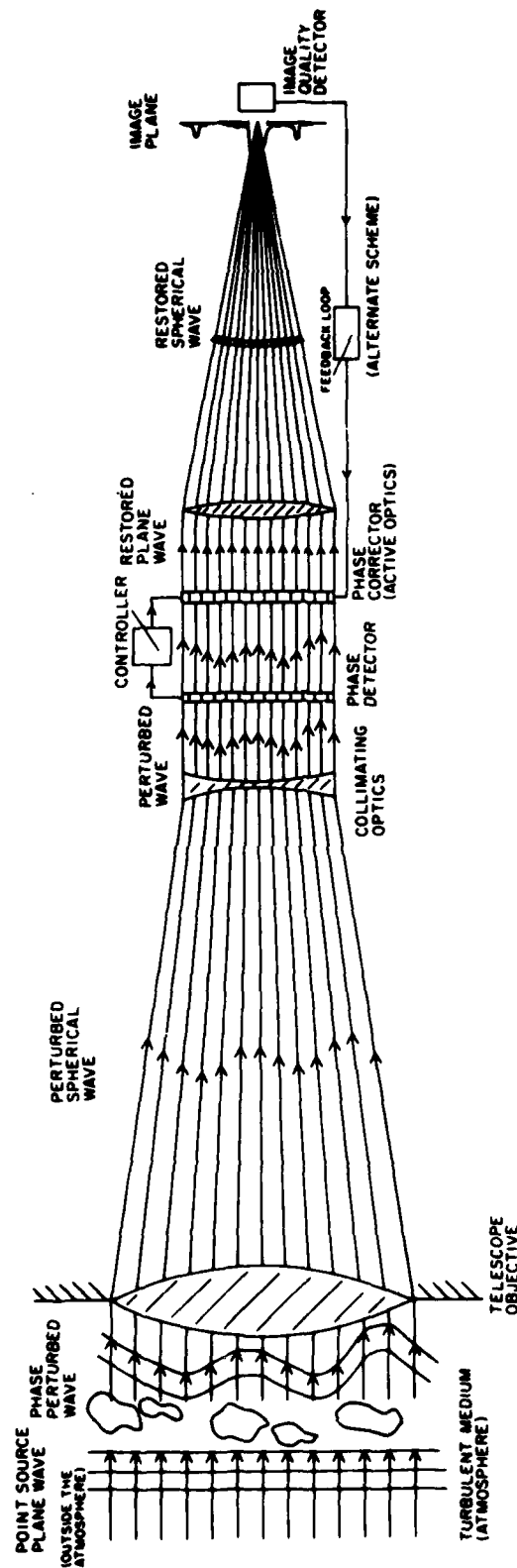
The averaged seeing-corrected power spectrum is then processed further to remove the seeing and detector-telescope transfer functions, and the result is then filtered and iteratively cleaned to improve its "reality" properties.

The final power spectrum is then combined with the phase factors (computed either from the averaged phase-unwrapped angles or averaged K-T ratios), and the result is inverse-Fourier transformed to get a preliminary image. Such preliminary images usually have negative values in some pixels, so a Fienup algorithm is used to retouch them.

Currently these phase-retrieval and image reconstruction algorithms have only been applied to analogue mode data. Efficient, discrete-address phase accumulation methods have not yet been developed in view of the well-known sensitivity of phase retrieval methods to single frame signal-to-noise ratio.

## B. WAVEFRONT RECONSTRUCTION METHODS

A highly desirable imaging system is one requiring no post-detection processing. As first proposed by Babcock (1953,1958), a device is introduced into the optical path which detects in real time the atmospherically induced phase fluctuations. A second device introduces countering phase shifts to reconstruct an unperturbed wave. Figure 16 represents two approaches to this problem. The simplest conceptual design uses a device to measure image sharpness, possibly by maximizing high spatial frequency components. A feedback loop is coupled back to phase shifting optics, usually a mirror with a deformable surface, the "rubber mirror." Such mirrors are manufactured by ITEK Corporation and consist of a thin optical flat mated to a piezo-electric matrix which can be deformed point by point with an applied voltage. Different portions of the rubber mirror are moved to achieve maximum image sharpness. A more general scheme involves determining the point-by-point phase errors in the aperture plane. This information is then fed directly to the counteracting deformable optics. The phase error determination may be accomplished in several ways (Wyant 1975). A very successful method used by the ITEK Corporation is to introduce a shear in the incoming wavefront. The resulting interference pattern intensity profile may be read and interpreted to yield the phase errors to be corrected (Hardy et al., 1974). This method is qualitatively similar to methods used to determine phase differences in the K-T process. Active optical systems suffer from two limitations. First, atmospheric phase errors must be detected and corrected before they change. More importantly, the phase compensation is valid only over a portion of the isoplanatic patch where the phase errors are highly constant, perhaps less than 2 arc-seconds. These problems limit this method to relatively bright objects. To accomplish a large area reconstruction, as for the solar surface, requires each isoplanatic patch be reconstructed independently. One approach to the latter problem is to use multiple reconstruction loops for each isoplanatic patch, however this could become prohibitively expensive. An alternate approach to this problem is to reconstruct one isoplanatic area at a time, place the reconstructed area into an array processor and step the active optic device to repeat the process. Fast array processors and computers are



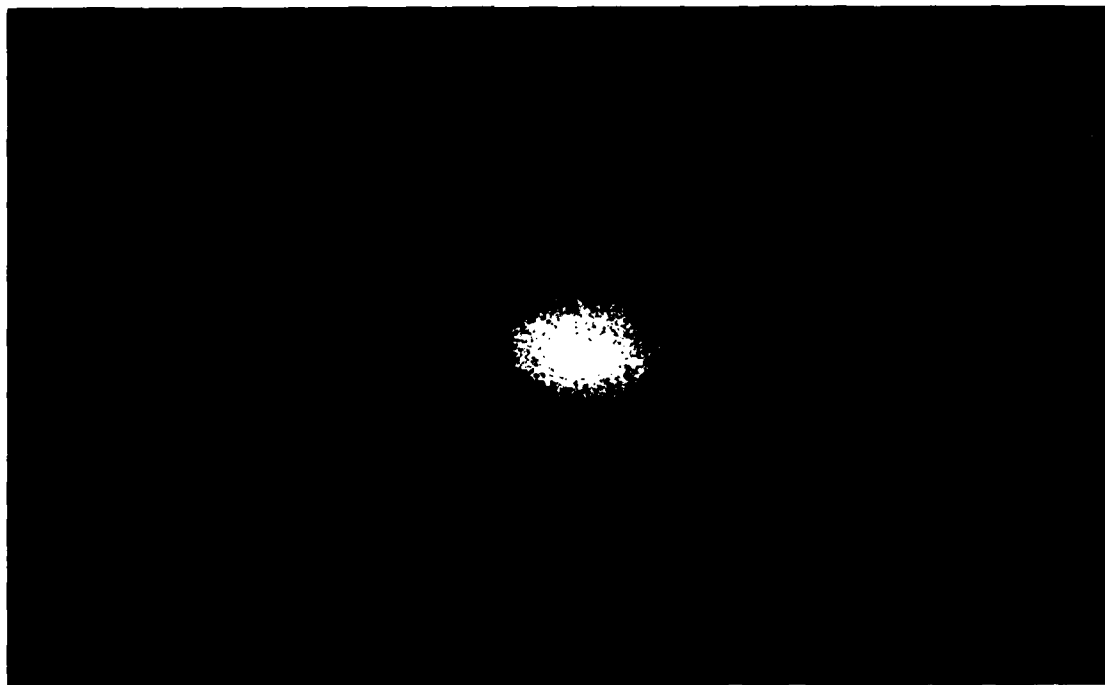
NOTE: Both an image sharpness scheme and a direct phase-detection system are shown.

Fig. 16. Two Types of Active Optical Systems

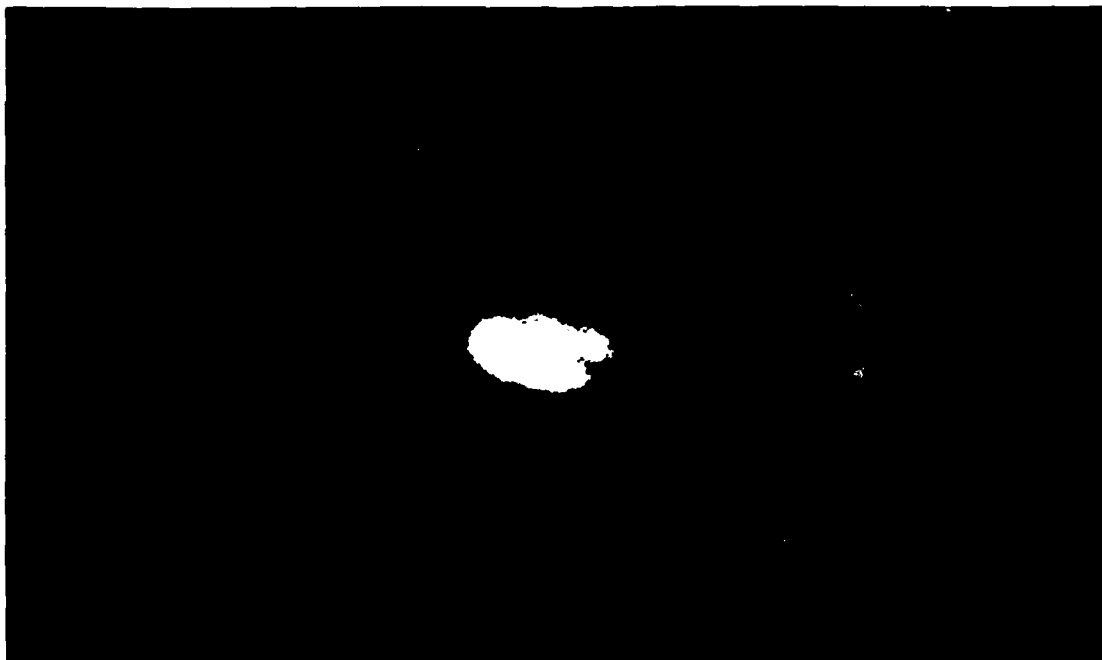
readily available to perform the image integration and processing. These limitations and requirements make active optics most applicable for solar image work.

To test and demonstrate active optics on solar images, AFGL performed a test of the ITEK active optics system (Hardy et al., 1976). The ITEK device uses a shearing interferometer with array detectors to measure the atmospherically induced phase errors. A deformable mirror consisting of a thin optical surface mated to piezo-electric material supplies the movement to compensate for the phase errors. The ITEK test device has 21 independent phase correcting elements. As seen in Figure 17, the system worked well on stellar point sources, recovering a fully compensated diffraction-limited star image. The extended solar image presented a more difficult problem and the test was unsuccessful for the sun. The failure was attributed to a dramatic decrease in isoplanatic patch size during daytime seeing conditions. ITEK had modified its unit to cope with the smaller isoplanatic size, and a new series of tests produced somewhat better results. We note that each detector/corrector loop compensates for only one phase-constant area of the telescope aperture. With only 21 individual loops and an apparent daytime phase coherence length ( $r_0$ ) of about 3 cm, only about 20 cm of telescope aperture was usable. To compensate the full 72 cm aperture of the Sacramento Peak Tower Telescope requires several hundred detector/corrector loops. Using a preliminary ITEK estimate of \$5000 per loop, a full system costs nearly \$1 million, not including the array processor hardware for large area reconstruction which we estimate to cost an additional \$300,000. Clearly such systems are costly compared to speckle methods. However, the active optics approach with a real-time correction and the ability to make available a corrected image for further analysis, in a spectrograph for example, has immense appeal for solar physics. Its potential is so great for solar physics that the active optics cost is well-justified and is being actively pursued by AFGL.

As pointed out, active optics systems can provide diffraction-limited images only for bright targets. Limiting brightness is set by the system's ability to detect and correct the atmospheric phase error before the error can change significantly. Using a simple form of active optics system, we can



a



b

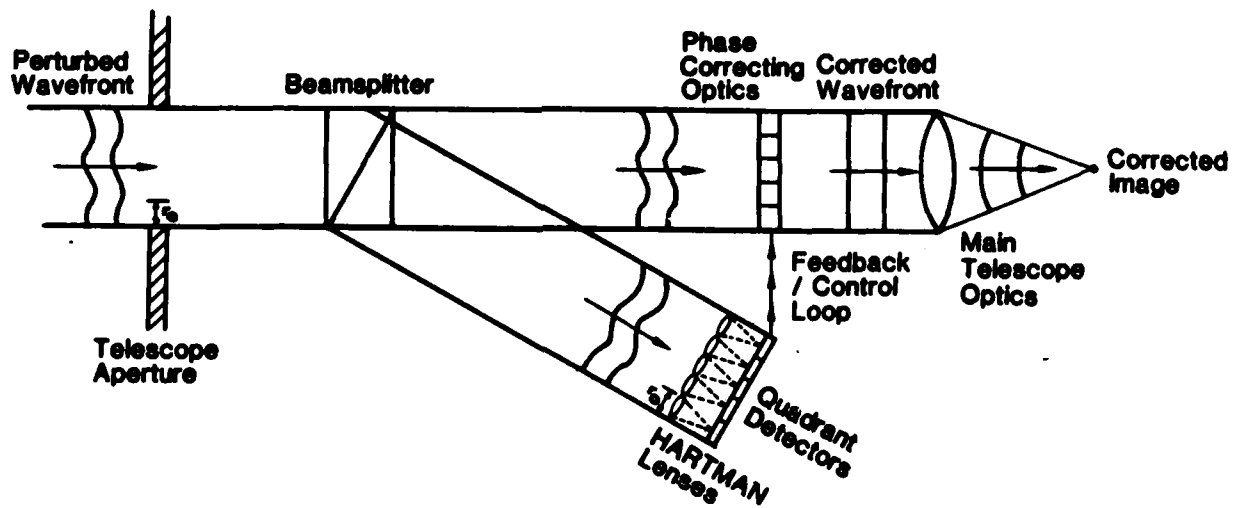
NOTE: A 50-cm aperture on the Sacramento Peak Power telescope was used. The uncompensated image is shown in "a"; an improvement to about 0.2 arc-second expected in a diffraction-limited case is nearly reached in "b."

Fig. 17 Results of ITEK Rubber Mirror Test on Point Source Stars

estimate what the limits might be. We propose using the "Hartman" test method for detecting atmospheric phase errors (cf Wyant, 1975). This method, illustrated in Figure 18, treats each small  $r_0$  phase coherent patch of the telescope aperture separately. We will assume for this discussion that  $r_0 = 10$  cm. Each  $r_0$  patch is imaged separately with a small 10 cm "lens." Since the  $r_0$  patch is phase coherent, each independent patch differs from its neighbors only by a DC phase offset or "piston" term and a phase error slope or "tilt" across the patch. Consequently, the images from each 10 cm lens will be identical except for a positional offset relative to the centerline of the 10 cm lens system. This offset is directly translatable into the tilt and piston offset for the 10 cm patch. Thus, to measure and correct the phase error, one needs only to use a simple quadrant detector in the 10 cm lens image in a closed loop with an active optics element. The limiting requirement is clearly to record enough photons in a 10 cm patch during the integration period before the atmosphere changes so that the image displacement can be accurately defined and corrected.

To correct for a phase error, we assume that it would be necessary to measure that error to within  $\pm\pi/6$  radians ( $30^\circ$ ). This translates to locating the center of each Hartman lens image to better than 8 percent of its diameter. If we detect  $n$  photons per image, then simple gaussian statistics imply that the center of the image may be located to  $\pm 1/\sqrt{n}$  of the image diameter. Thus, about 150 photons are required to obtain the desired 8 percent diameter accuracy. System quantum efficiency for a good speckle system is about 10 percent per 100 Å bandpass (Hege et al., 1980). Thus, for a broadband active optics system with a 10 ms integration and cycle time, we would need photon arrival rates at the telescope of  $\sim 10^3/\text{cm}^2/\text{sec}$  to achieve  $\pi/6$  radian accuracy per Hartman loop ( $r_0 \sim 10$  cm) element, or about an 11th magnitude star. Reminding the reader that the comparison star must be within one isoplanetic patch, which we assume to be 3 arc-seconds, and finding that there are  $\sim$ ten 11th magnitude stars per square degree, we conclude that about  $10^{-5}$  of the sky would be observable with the active optics systems likely to be available.





NOTE: The atmospherically perturbed wave front enters the telescope aperture and the wave is split into two components, the majority of the light progressing toward the main telescope optics, the remainder entering the Hartman optics. Individual focusing elements,  $r_0$  in diameter, bring phase coherent subelements to independent foci. The displacement of each of these images from nominal centerline is detected by quadrant detectors and translated into phase error signals. These signals are sent to phase correcting optics which reconstruct an unperturbed wave front. The light is then brought to a focus by the main telescope optics to produce an image free from atmospherically induced degradation.

Fig. 18. Operation of Hartman Active Optics System

To expand the applicability of active optics systems, we suggest a compromise approach (Woolf 1981). If we use a phase detection arc correcting loop which averages over several individual  $r_0$  phase coherent patches, several advantages accrue: A fainter comparison star can be used, a larger isoplanatic patch is likely, and the atmospheric change time is longer. Against these advantages must be balanced the greatly decreased improvement in image quality. There is, therefore, a compromise instrument where nearly the entire sky might be observed with a suitable active optics comparison star available, and where a usable increase in resolution results. Such an instrument may then be coupled to some form of speckle-based image reconstruction to provide the most efficient image reconstruction system. An improvement in image quality brought about by a partial active optics system enhances further speckle processing since the same number of photons are concentrated into fewer "speckles," or more precisely, interference fringes.

N. Woolf (1981) has studied the optimum hybrid active optics/speckle configuration and determined isoplanatic angle size for a given active optics single element size ( $r_0$ ) assuming all turbulence is at one level in the atmosphere ( $\sim 3$  km height) and a standard atmospheric turbulence model. The same model and calculation coupled with an estimate of wind speed at that altitude provides an estimate of the atmospheric change time. Woolf (1981) concludes that an optimum system would have individual elements of 1.5 to 2.0 meters in diameter. A usable guide star (18-19th magnitude) would then be available within 2-3 arc-minutes of most objects in the sky. For a 1.5 to 2.0 meter element the isoplanatic angle (or more correctly for the larger element, the "aplanatic" angle) becomes 2-3 arc-minutes. Atmospheric change time increases to 0.2 sec making an 18th magnitude star a suitable comparison source for existing active optics systems. The net active optics image improvement is estimated to be 25 percent over an uncorrected system. This is about a factor of two improvement in number of photons per speckle, indicating the good potential utility of a hybrid system. Since this size is similar to the individual mirror size (1.8 m) for the Arizona/Smithsonian Multiple Mirror Telescope, that instrument is ideal as a test for these ideas.

## V. SUMMARY

The atmosphere degrades images of objects observed through it. The basis of this degradation is the introduction of phase shifts in an incoming light-wave by passage through atmospheric regions with variable index of refraction due to small scale density inhomogeneities largely due to temperature variations. The phase errors, coherent over less than 10 cm, change in less than 0.05 second and effectively reduce all telescope resolutions to the 1 arc-second value appropriate to a 10 cm instrument. In 1970, Labeyrie pointed out that short exposure "speckle" photos freeze this turbulence and convert large telescopes to a form of multiple aperture interferometer. Using sophisticated Fourier descriptions of this optical process, various workers have shown during the 1970s that speckle photos contain extractable high frequency angular scales down to the diffraction limit of the largest existing telescopes. Numerous investigators have used this result to derive the size and shape of astronomical objects as small as 0.02 arc-second by computing the instantaneous power spectrum of the speckle photos. With new calibration methods and high efficiency digital recording systems capable of recording the arrival of most incoming photons, sizes of objects fainter than +15 magnitudes may be obtained with 5% accuracy. The major task facing us now is to reconstruct images free from atmospheric degradations rather than just get sizes and shapes. In 1975, Lynds et al. showed that images of bright stars were directly obtainable from speckle photos. For more general image reconstruction, the power spectrum used to determine angular sizes must be supplemented with Fourier phases. Sophisticated statistical techniques to get the phase from speckle photos directly have been developed by Knox and Thompson (1974) but are highly noise sensitive and limited to bright objects like the sun. Recently, a promising method developed by Fienup (1978) was successfully applied to derive phases for faint astronomical targets. The technique relies on an iterative processing using the true power spectrum derived as described above as an input. The method is insensitive to noise and shows that actual diffraction-limited images can be reconstructed for objects fainter than +15 magnitudes. Our recent work shows that a combination of phase retrieval and

image reconstruction methods should produce optimal images. Active optics ("rubber mirror") systems exist which compensate for atmospheric degradation in real time. A unit built by the ITEK Corporation was tested on astronomical targets. Despite its high cost and limitation to bright objects, such devices are ideal for solar work as they provide real-time corrected images for input into other conventional analyzing instruments; however, they appear to be totally inappropriate for faint object systems. We suggest that an optimal system for large-aperture, faint-object diffraction-limited image recovery will utilize all available technologies.

## REFERENCES

1. Babcock, H. W. 1953, Pub. Ast. Soc. Pac. 65, 229.
2. Babcock, H. W. 1958, J. Opt. Soc. Am. 48, 500.
3. Bates, R. H. T., Milner, M. O., Lund, G. I., and Seager, A. D. 1978, Opt. Commun. 26, 22.
4. Boksenberg, A. 1978, Optical Telescopes of the Future, Conf. Proc. 1977 Dec (Geneva 23: ESO c/o CERN) p. 497.
5. Bracewell, R. 1965 (1978 2nd Edition), The Fourier Transform and its Application (New York: McGraw Hill).
6. Brault, J. J. and White, O. R. 1971, Astron. and Astrophys. 13, 169.
7. Bruck, Y. M. and Sodin, L. G. 1979, Opt. Comm. 30, 304.
8. Cocke, W. J. 1980, Proc. SPIE 231-11, submitted to J. Opt. Soc. Am.
9. Dainty, J. C. 1975, Stellar Speckle Interferometry in Laser Speckle and Related Phenomena (Berlin: Springer-Verlag).
10. Gezari, D. Y., Labeyrie, A., and Stachnik, L. V. 1972, Ap. J. (Letters) 173, L1.
11. Gerchberg, R. W. and Saxton, W. O. 1972, Optik 35, 237.
12. Hardy, J. W. 1978, Private Communication.
13. Hardy, J. W., Lefebvre, J. E., and Koliopoulos, C. L. 1977, J. Opt. Soc. Am. 67, 360.
14. Hege, E. K., Hubbard, E. N., and Strittmatter, P. A. 1980, Proc. SPIE 264, 29.
15. Hubbard, G., Worden, S. P., Strittmatter, P. A., Hege, E. K., and Reed, M. 1978, Digital Speckle Interferometry to Measure the Angular Diameters of Faint Objects, in IAU Colloquium #50 (Amsterdam: Reidel).
16. Hubbard, G., Hege, K., Reed, M. A., Strittmatter, P. A., and Woolf, N. O. 1979, Astron. J. 84, 1437.
17. Huiser, A. M. J. and van Toorn, P. 1980, Opt. Letters 5, 499.

18. Knox, K. T. 1975, Diffraction Limited Imaging with Astronomical Telescopes, Ph.D. Dissertation, The University of Rochester.
19. Knox, K. T. and Thompson, B. J. 1974, Ap. J. (Letters) 193, L45.
20. Korff, D. 1973, J. Opt. Soc. Am. 63, 971.
21. Korff, D., Dryden, G., and Miller, M. G. 1972, Optics Comm. 5, 187.
22. Labeyrie, A. 1978, Am. Rev. Astr. and Astrophys. 16, 77.
23. Liu, C. Y. C. and Lohman, A. W. 1973, Optics Comm. 8, 372.
24. Lynds, C. R., Worden, S. P., and Harvey, J. W. 1976, Ap. J. 207, 174.
25. McAlister, H. A. 1977, Ap. J. 215, 159.
26. McGlamery, B. L. 1971, in Astronomical Use of Television Type Image Sensors, NASA SP 256, p. 167.
27. Mertz, L. N. 1979, Appl. Opt. 18, 611.
28. Michelson, A. A. 1921, Ap. J. 51, 257.
29. Miller, M. G., Schneidman, A., and Keller, P. E. 1973, Ap. J. (Letters) 186, L91.
30. Nisensen, P., Stachnik, R. V., and Noyes, R. W. 1980, Private Communication.
31. Stachnik, R. V., et al. 1977, Nature 266, 149.
32. Strittmatter, P. A. 1980, Proc SPIE 243, 75.
33. Wang, C. P. 1974, Opt. Comm. 10, 253.
34. Weigelt, G. P. 1978, Appl. Opt. 17, 2660.
35. Weigelt, G. P. 1979, Optica Acta 26, 1351.
36. Welter, G. L. and Woren, S. P. 1978, J. Opt. Soc. Am. 68, 1271.
37. Wiener, N. 1949, Extrapolation and Smoothing of Stationary Time Series (New York: Wiley).
38. Woolf, N. J. 1981, University of Arizona Preprint.
39. Worden, S. P. 1979, Vistas in Astron. 20, 301.
40. Worden, S. P. and Stein, M. K. 1979, Astron. J. 84, 130.

41. Worden, S. P., Stein, M. K., Schmidt, G. D., and Angle, J. R. P. 1971, Icarus 32, 450.
42. Wyant, J. C. 1974, Imaging in Astronomy, Conference Preprints, Boston, June 1975.